

NASA TECHNICAL NOTE



NASA TN D-6807

2.1

NASA TN D-6807



LOAN COPY: RE
AFWL (DO
KIRTLAND AFB

JOULE-THOMSON INVERSION CURVES AND RELATED COEFFICIENTS FOR SEVERAL SIMPLE FLUIDS

*by Robert C. Hendricks, Ildiko C. Peller,
and Anne K. Baron*

*Lewis Research Center
Cleveland, Ohio 44135*





0133484

1. Report No. NASA TN D-6807	2. Government Accession No.	3. Recipient's Catalog No.	
4. Title and Subtitle JOULE-THOMSON INVERSION CURVES AND RELATED COEFFICIENTS FOR SEVERAL SIMPLE FLUIDS		5. Report Date July 1972	6. Performing Organization Code
		8. Performing Organization Report No. E-6786	10. Work Unit No. 113-31
7. Author(s) Robert C. Hendricks, Ildiko C. Peller, and Anne K. Baron		11. Contract or Grant No.	
		13. Type of Report and Period Covered Technical Note	
9. Performing Organization Name and Address Lewis Research Center National Aeronautics and Space Administration Cleveland, Ohio 44135		14. Sponsoring Agency Code	
		12. Sponsoring Agency Name and Address National Aeronautics and Space Administration Washington, D. C. 20546	
15. Supplementary Notes			
16. Abstract <p>The equations of state (PVT relations) for methane, oxygen, argon, carbon dioxide, carbon monoxide, neon, hydrogen, and helium were used to establish Joule-Thomson inversion curves for each fluid. The principle of corresponding states was applied to the inversion curves, and a generalized inversion curve for fluids with small acentric factors was developed. The quantum fluids (neon, hydrogen, and helium) were excluded from the generalization, but available data for the fluids xenon and krypton were included. The critical isenthalpic Joule-Thomson coefficient μ_c was determined; and a simplified approximation $\mu_c \approx T_c/6P_c$ was found adequate, where T_c and P_c are the temperature and pressure at the thermodynamic critical point. The maximum inversion temperatures were obtained from the second virial coefficient (maximum (B/T)).</p>			
17. Key Words (Suggested by Author(s)) Thermodynamics		18. Distribution Statement * Unclassified - unlimited	
19. Security Classif. (of this report) Unclassified	20. Security Classif. (of this page) Unclassified	21. No. of Pages 60	22. Price* \$3.00

JOULE-THOMSON INVERSION CURVES AND RELATED COEFFICIENTS FOR SEVERAL SIMPLE FLUIDS

by Robert C. Hendricks, Ildiko C. Peller, and Anne K. Baron

Lewis Research Center

SUMMARY

The pressure-volume-temperature (PVT) relations for several fluids (methane, nitrogen, oxygen, argon, carbon dioxide, neon, carbon monoxide, fluorine, hydrogen, and helium) have been used to study the behavior of the isenthalpic Joule-Thomson coefficient and in particular the inversion curve. Some attention is also given to Joule-Thomson refrigerators and liquifiers. For the fluids methane, nitrogen, oxygen, argon, carbon dioxide, and neon the calculations involved extrapolation of the equation of state to high pressure and temperature. In all cases the PVT extrapolations and the derivatives $(\partial P/\partial T)_\rho$ and $(\partial P/\partial \rho)_T$, where ρ is density, appeared to be natural extensions of the lower pressure and temperature results. These results for nitrogen were compared to the PVT relation of Coleman and Stewart, which was developed for nitrogen and covers pressures to 1000 atmospheres and temperatures to 1000 K. The comparisons were quite favorable.

From these results a Joule-Thomson inversion curve was calculated for each fluid. The curves were compared to existing data with favorable results for all but carbon monoxide, where sizable deviations from the data were noted for temperatures above a reduced temperature T_R of 3. An approximation for the critical isenthalpic Joule-Thomson coefficient μ_c was developed. This simple formula, $\mu_c = T_c/6P_c$, was found to be in good agreement with the data of Roebuck and Osterberg and Coleman and Stewart for nitrogen. Reduced Joule-Thomson data were determined for eight fluids and plotted as a function of reduced temperature for various isobars (reduced pressures).

The inversion curve and the isothermal Joule-Thomson coefficient are shown to comply with the principle of corresponding states. The isenthalpic Joule-Thomson variable does not. Nevertheless, the reduced inversion curves are useful when data are absent and for grouping data in fluid-to-fluid comparisons.

The inversion temperature and the Boyle temperature as calculated from the second virial coefficient B were also found to be in agreement with values found in the literature.

Finally, a revised form of the generalized inversion curve is presented. The fluids helium, hydrogen, and neon were not included in the generalization because of their quantum effects. Carbon dioxide was also excluded from the generalization because of its high acentric factor. Available low-temperature-fluorine data were included.

INTRODUCTION

Joule-Thomson expansion is widely used for liquification of gases and for refrigeration. There are no moving parts, maintenance is minimal, and reliability is high. Joule-Thomson expansion is usually used in the lowest temperature portion of a liquification or refrigeration cycle; however, when coupled with a pump, a complete cycle is formed. The Joule-Thomson liquification and refrigeration processes are discussed in appendix D along with some indication of how the figure of merit (cost of producing a unit of liquid or cooling) influences the cycle design. It should be noted that the maximum refrigeration or liquification does not correspond to minimum cost. A variety of specific cooling and liquification applications can be found in reference 1.

Under certain conditions a Joule-Thomson expansion will produce heating rather than cooling; consequently, determining these conditions is important to the design of cryogenic equipment. In the Joule-Thomson experiment, the gas is expanded isenthalpically through a porous plug, and the slope of the isenthalpic curve (constant H) in the pressure-temperature (P - T) plane is called the Joule-Thomson coefficient μ

$$\mu = \left(\frac{\partial T}{\partial P} \right)_H$$

(All symbols are defined in appendix F.) The unique locus of points where the isenthalp is a maximum is called the inversion curve. Thus, for a certain temperature, there exists a pressure beyond which $\mu < 0$ and isenthalpic expansion causes a temperature rise. However, at lower pressures, $\mu > 0$ and cooling results from isenthalpic expansion. The maximum isenthalpic cooling occurs when conditions on the high-pressure side of the plug (or valve) fall on the inversion locus (appendix D).

While the Joule-Thomson effect has been experimentally determined for several fluids (e.g., refs. 2 to 7), it is not only a very difficult experiment but requires precise PVT data for cross interpolation. Thus, when accurate experimental data for a particular gas are either inadequate or nonexistent, it becomes necessary to estimate the inversion curve. While the principle of corresponding states has been applied to the inversion curve by several authors (e.g., refs. 8 and 9), Gunn, Chueh, and Prausnitz (ref. 10) reexamined both the experimental and calculated Joule-Thomson "data" for argon, xenon, nitrogen, carbon monoxide, methane, ethylene, neon, helium, hydrogen, and some mixtures (see also appendix A). Quantum gases (helium, hydrogen, and neon) do not follow the corresponding states principle except at high temperatures and, consequently, were correlated separately. The inversion curve for the remaining gases

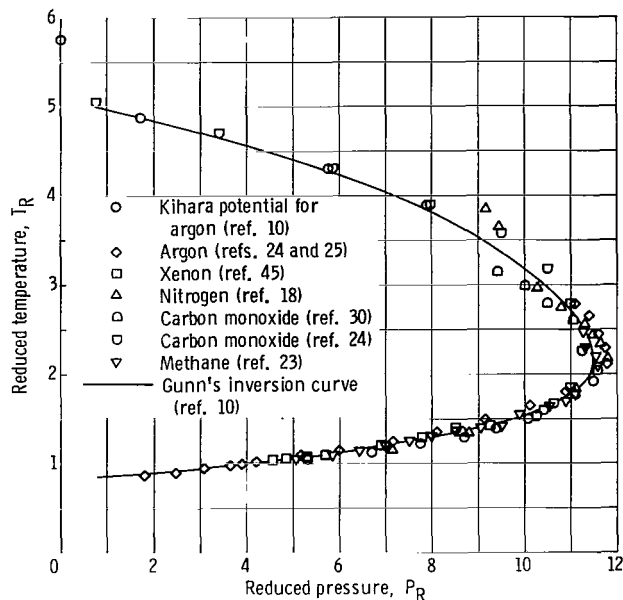


Figure 1. - Generalized reduced inversion curve for several corresponding states fluids as determined by Gunn, Chueh, Prausnitz (ref. 10).


(fig. 1) was well represented in terms of reduced temperature ($T_R = T/T_c$) and reduced pressure ($P_R = P/P_c$) by

$$P_R = \sum_{i=0}^5 \alpha_i T_R^i$$

α_0	α_1	α_2	α_3	α_4	α_5
-36.275	71.598	-41.567	11.826	-1.6721	0.091167

Gunn, Chueh, and Prausnitz (ref. 10) also concluded that Joule-Thomson coefficients calculated with an accurate equation of state should be more accurate than those measured experimentally. It must be remembered that accuracy in measuring the pressure drop in an isenthalpic experiment and interpolating these data to determine $(\partial T/\partial P)_H$ is very difficult to obtain.

Recently, accurate PVT data on methane and oxygen have been acquired (refs. 11 and 12). Coleman and Stewart (ref. 13) have reexamined all the available nitrogen data and presented an equation of state that is valid over a considerable range of pressure. Bender (ref. 14) reported an accurate equation of state for five fluids: methane, nitro-



gen, oxygen, argon, and carbon dioxide. Hendricks, Baron, Peller, and Pew (ref. 15) developed a computer program to calculate the thermodynamic and transport properties for eight fluids. The primary equation selected in this program was the Bender equation, because it covered five fluids of considerable interest with a consistent curve fit. Carbon monoxide, neon, and helium were also included in reference 15 by using equations formulated at NBS-Boulder (see ref. 15). In addition, the Coleman and Stewart equation for nitrogen (ref. 13), because of its extended pressure range, was also included in the program of reference 15.

For most fluids, neither the equation of state nor the data cover the extreme pressure-temperature ranges required to obtain the Joule-Thomson curve and related results. The only equation used in reference 15 which was originally fit to the very high pressures required to determine the inversion curve was the Coleman and Stewart equation for nitrogen (ref. 13). Consequently, the first topic of this report is a discussion of the validity of the PVT results obtained when the equations of state for the eight fluids as defined in reference 15 are extrapolated to the high pressure required to compute the Joule-Thomson inversion curve.

Second, by using the computer program of reference 15, the work of reference 10 is extended to present inversion curves and related Joule-Thomson results for the fluids methane, nitrogen, oxygen, carbon dioxide, argon, carbon monoxide, neon, and helium. Limited results for hydrogen, fluorine, and some noble gases are also included.

The next topic covered is the calculation of inversion temperatures by using the second virial coefficient of the equation of state programmed in reference 15.

Finally, the principle of corresponding states as applicable to the inversion curve and the critical isenthalpic Joule-Thomson coefficient is discussed.

HIGH-PRESSURE PVT EXTENSIONS

In order to extrapolate Bender's equation of state (ref. 14) to higher pressures and temperatures, it is first necessary to examine the extended isochores. The numerical values of the extended isochores for each fluid of figure 2 were based on the following increments of the critical isochore: $0.5 \rho_c$, $1.0 \rho_c$, $1.25 \rho_c$, $1.5 \rho_c$, $2.0 \rho_c$, $2.5 \rho_c$, and $3.0 \rho_c$. The isochores of figure 2 are bounded above by a pressure of 100 MN/m^2 and from the right by a temperature around 600 K. While these bounds may at first seem arbitrary, they were established to encompass most of the Joule-Thomson loci and in the case of nitrogen to compare the extrapolated isochores as predicted by Bender (ref. 14) to those predicted by Coleman and Stewart (ref. 13).

The equations of state for the fluids methane, nitrogen, oxygen, argon, carbon diox-

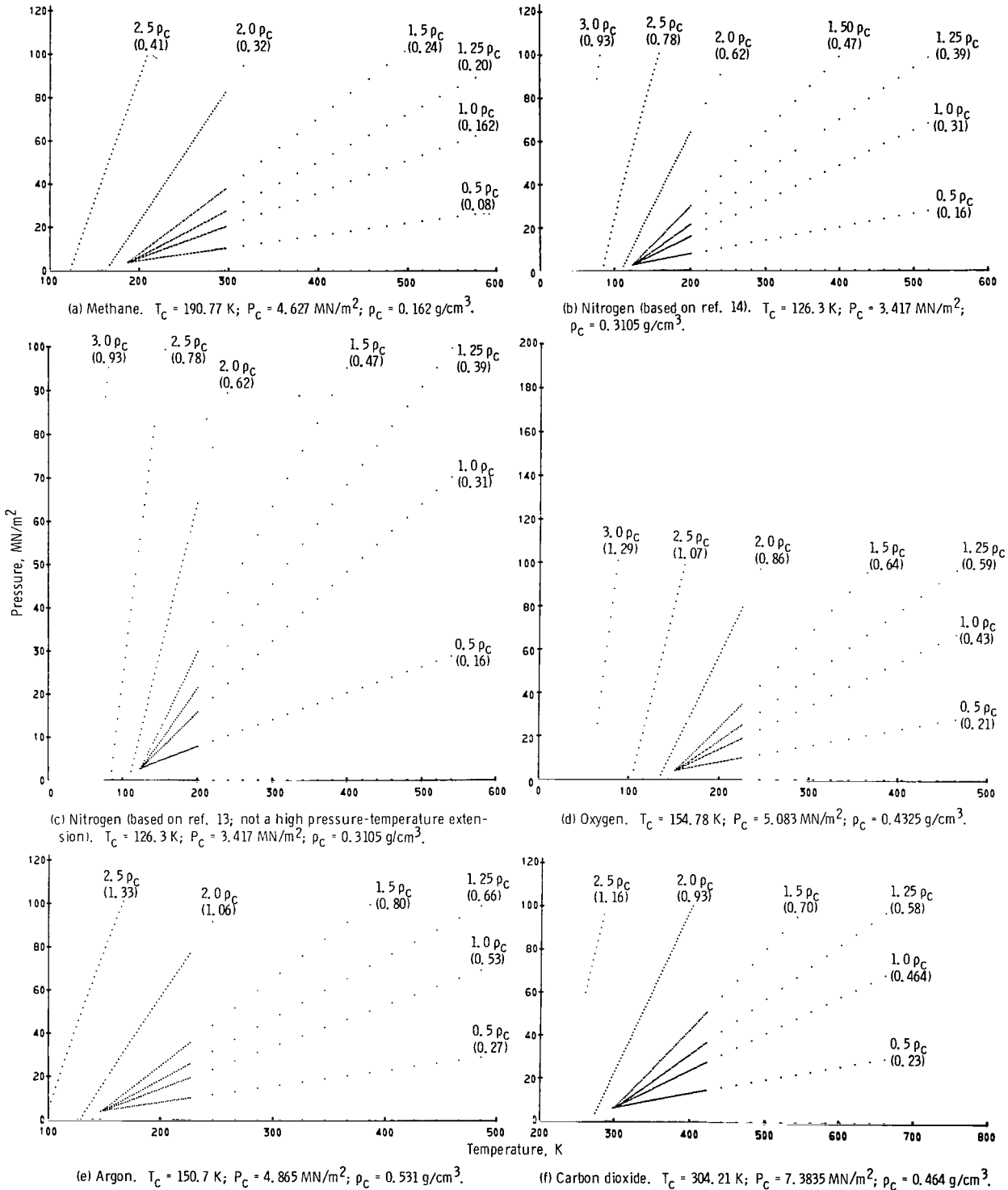
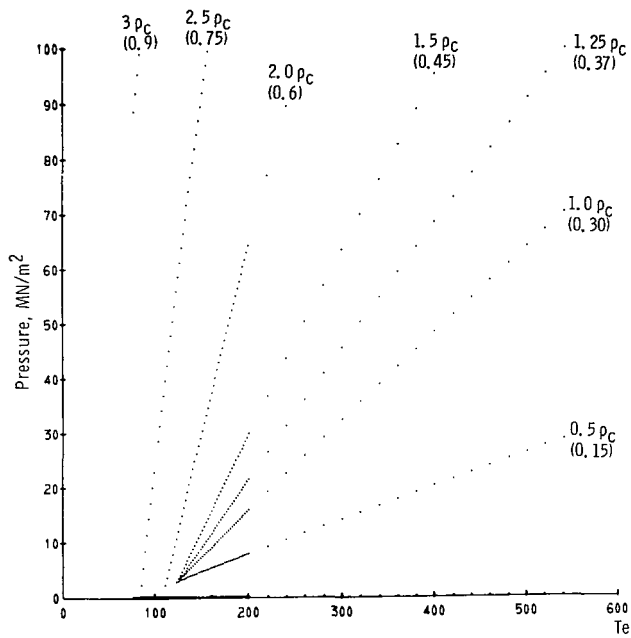
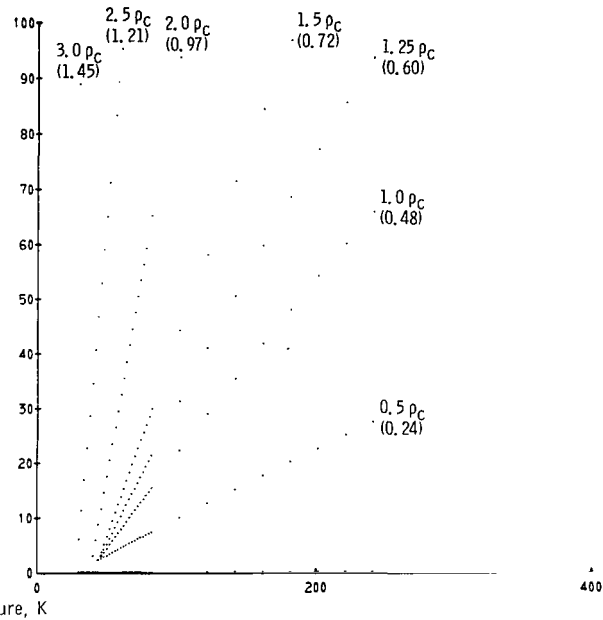


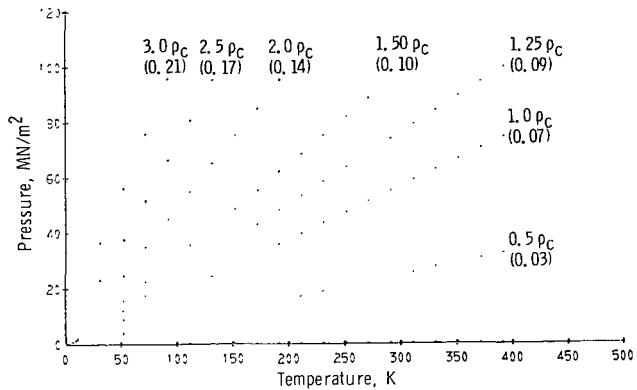
Figure 2. - PVT extensions along selected isochores for several fluids as calculated from reference 15, for various values of critical temperature T_C , critical pressure P_C , and critical density ρ_C .



(g) Carbon monoxide. $T_C = 132.91 \text{ K}$; $P_C = 3.4986 \text{ MN/m}^2$; $\rho_C = 0.2997 \text{ g/cm}^3$.



(h) Neon. $T_C = 44.4 \text{ K}$; $P_C = 2.6537 \text{ MN/m}^2$; $\rho_C = 0.483 \text{ g/cm}^3$.



(i) Helium. $T_C = 5.2 \text{ K}$; $P_C = 0.22764 \text{ MN/m}^2$; $\rho_C = 0.0693 \text{ g/cm}^3$.

Figure 2. - Concluded.

ide, carbon monoxide, and neon¹ were all fitted for pressures less than 40 MN/m², and that for helium for pressures less than 10 MN/m² (ref. 15). Nevertheless, the extrapolated isochores appear linear, continuous, and a natural extension from the lower pressure regime.

The slopes $(\partial P/\partial T)_\rho$ as presented in figure 3 indicate the linearity of the isochores. In general, the $(\partial P/\partial T)_\rho$ curves are nearly constant for densities to $\rho/\rho_c \approx 2$. However, at higher densities, that is, ρ/ρ_c of 2.5 and 3.0, the $(\partial P/\partial T)_\rho$ exhibits a high degree of curvature at low temperatures and tends toward a constant at higher temperatures.

The derivatives $(\partial P/\partial \rho)_T$, for various fluids, are not as easily compared. However, similar trends were noted for densities to ρ/ρ_c of approximately 2 (perhaps 2.5), even though quantitative trends were not established.

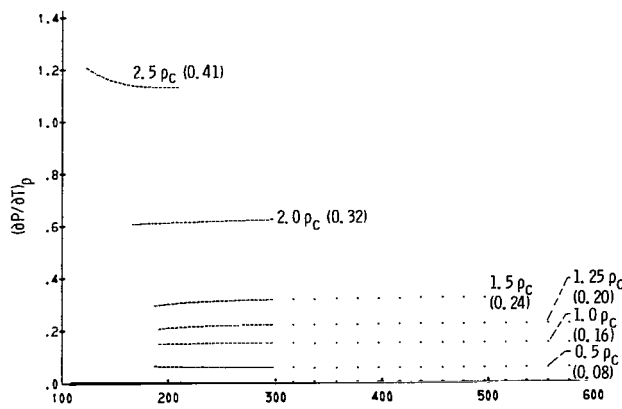
Due to the linear nature of the isochores in the P-T plane, the behavior of these derivatives is not unusual; and, as such, one would expect the extrapolated PVT results, in the absence of data, to be fairly good. A second reason for investigating the behavior of these derivatives is that they are used in the calculation of the Joule-Thomson coefficient.

The Coleman-Stewart equation of state for nitrogen (ref. 13) is valid to 100 MN/m² and 1000 K (this region includes the inversion curve). The extrapolated values of Bender's equation in figures 2(b) and 3(b) for nitrogen should agree with those calculated by using the Coleman-Stewart equation, in order to have greater confidence in the extrapolated results.

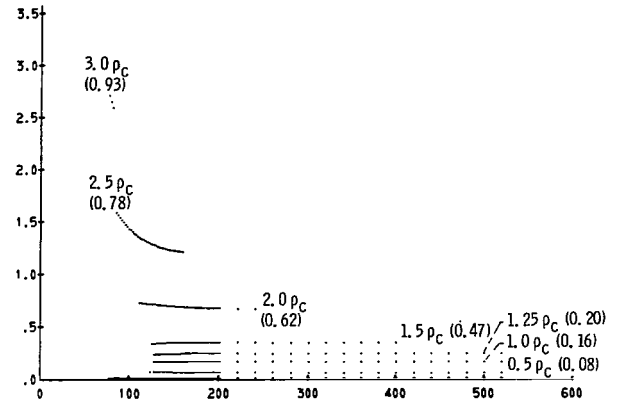
Apart from a slight shift of the high-density isochore as shown in figure 4, the isochores calculated by the two techniques are the same. In general, $(\partial P/\partial T)_\rho$, as calculated from references 13 and 14 by reference 15, are in good agreement (fig. 5).

In view of these results, one can expect the extrapolated PVT results to be a reasonable approximation to high-pressure data (when it becomes available).

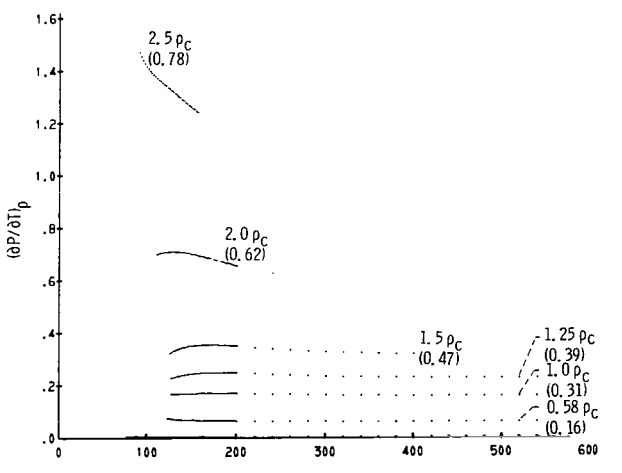
¹Preliminary Joule-Thomson points for fluorine are also presented; however, due to some unexpected curvature in the isochores and deviations in the enthalpy calculation, the J-T locus was not calculated herein.



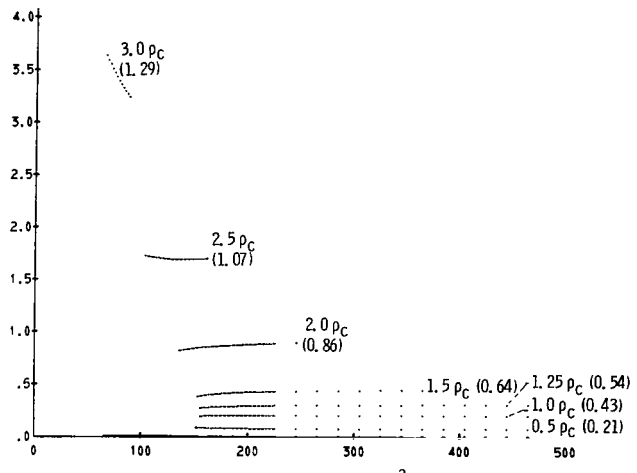
(a) Methane. $\rho_C = 0.162 \text{ g/cm}^3$.



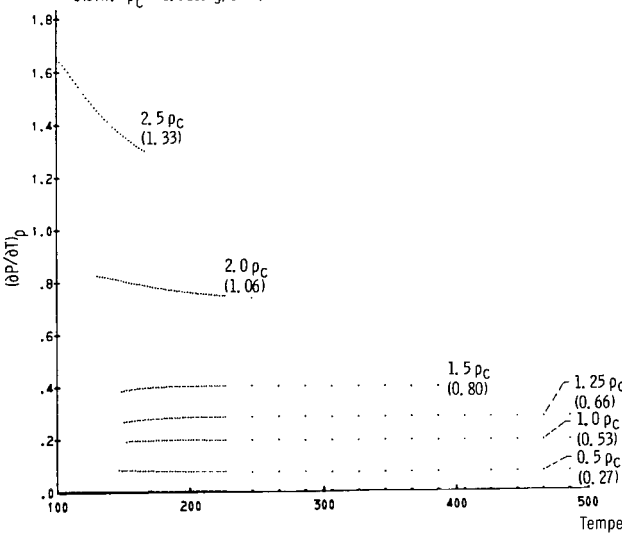
(b) Nitrogen (based on ref. 14). $\rho_C = 0.3105 \text{ g/cm}^3$.



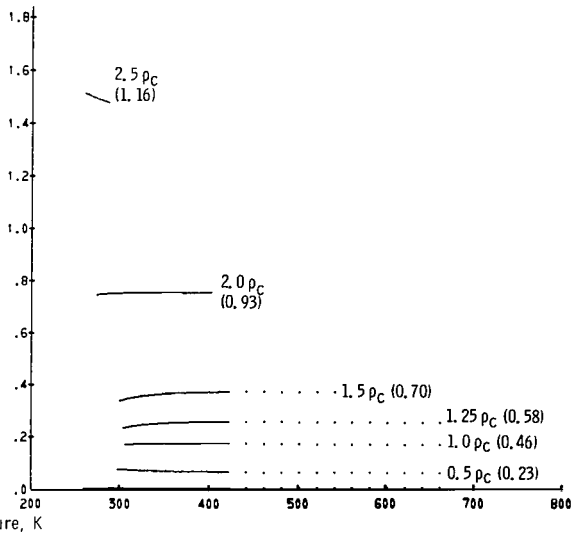
(c) Nitrogen (based on ref. 13; not a high pressure-temperature extension). $\rho_C = 0.3105 \text{ g/cm}^3$.



(d) Oxygen. $\rho_C = 0.4325 \text{ g/cm}^3$.

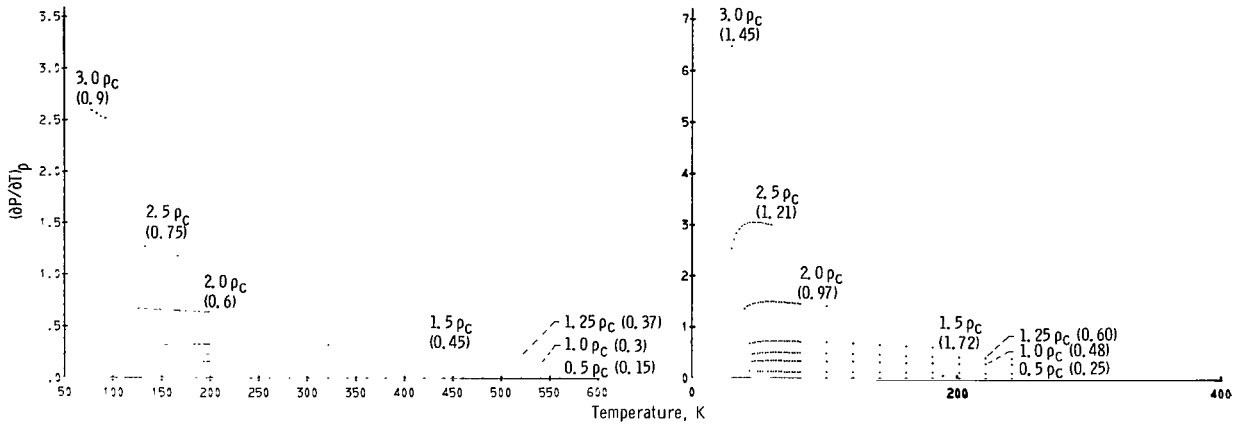


(e) Argon. $\rho_C = 0.531 \text{ g/cm}^3$.



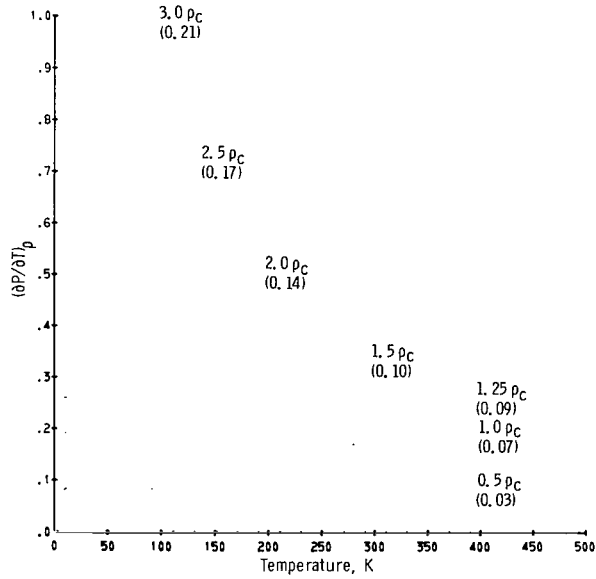
(f) Carbon dioxide. $\rho_C = 0.464 \text{ g/cm}^3$.

Figure 3. - Partial derivative $(\partial P/\partial T)_p$ as calculated from PVT extensions for selected isochores (ref. 15), for various critical densities ρ_C .



(g) Carbon monoxide. $\rho_C = 0.2997 \text{ g/cm}^3$.

(h) Neon. $\rho_C = 0.483 \text{ g/cm}^3$.



(i) Helium. $\rho_C = 0.0693 \text{ g/cm}^3$.

Figure 3. - Concluded.

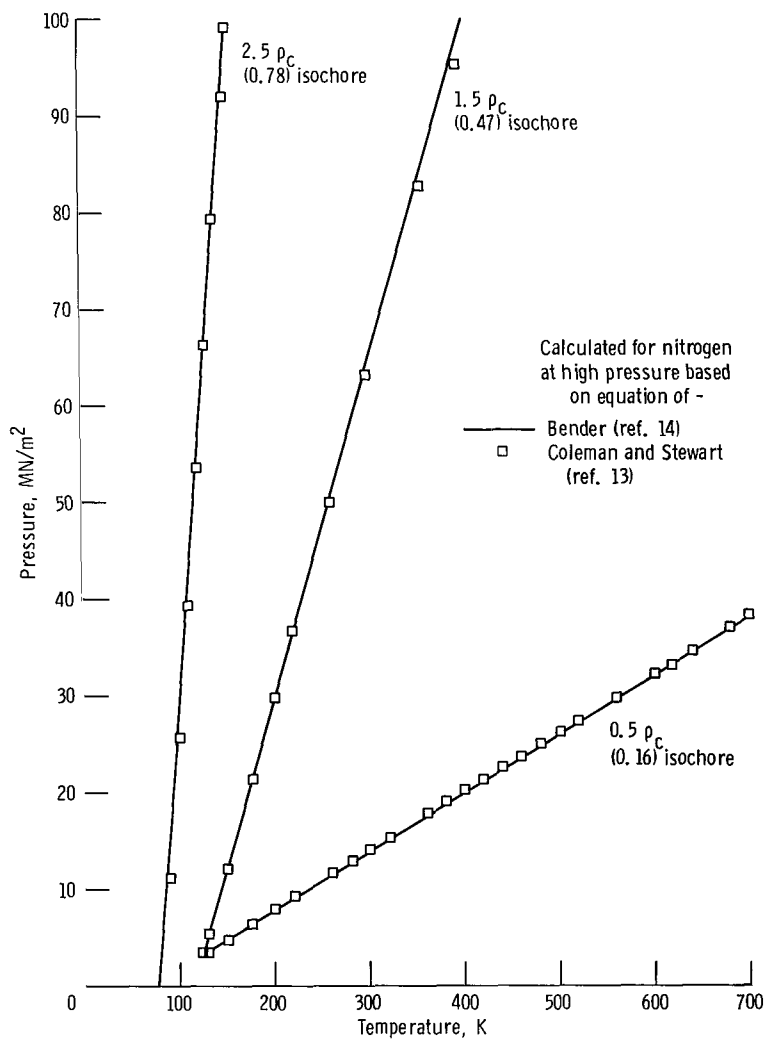


Figure 4. - Comparison of pressure-temperature plane for selected isochores based on reference 13 and the extended PVT results based on reference 14. Critical density, ρ_c , 0.3105 g/cm³.

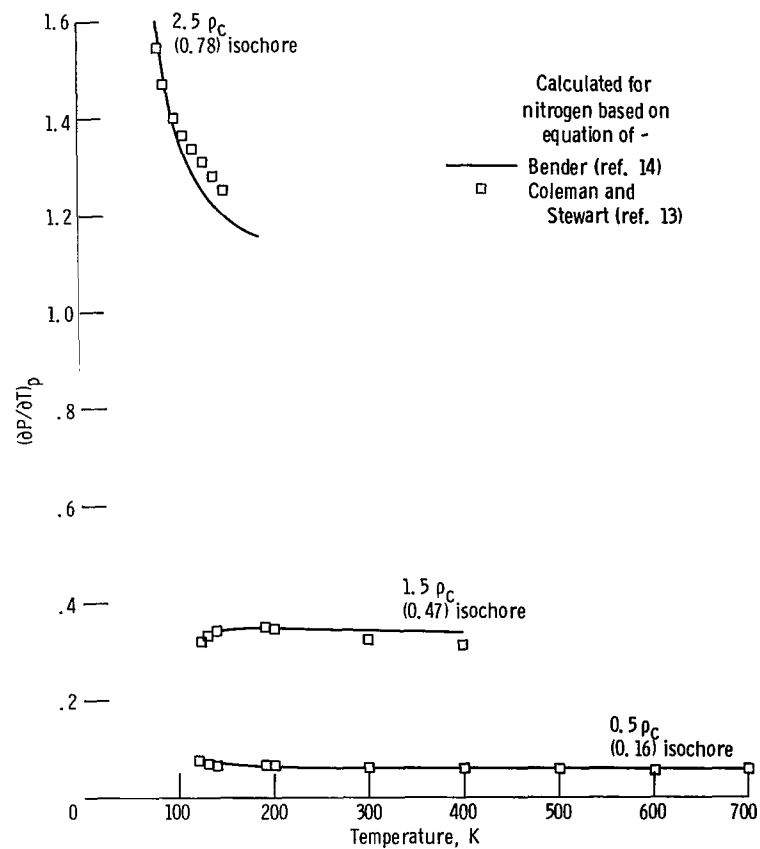


Figure 5. - Comparison of partial derivative $(\partial P / \partial T)_\rho$ based on reference 13 and the extended PVT results based on reference 14. Critical density, ρ_c , 0.3105 g/cm³.

JOULE-THOMSON EFFECTS

Inversion Curves

The isenthalpic Joule-Thomson coefficient, defined as the slope of an isenthalp in the T-P plane, can be written as

$$\mu = \left(\frac{\partial T}{\partial P} \right)_H = \frac{1}{\rho C_p} \left[\frac{T}{\rho} \frac{\left(\frac{\partial P}{\partial T} \right)_\rho}{\left(\frac{\partial P}{\partial \rho} \right)_T} - 1 \right] \quad (1)$$

The inversion curve is defined as the locus of maxima of these isenthalps in the T-P plane. This locus of points, where $\mu = 0$, can be calculated by determining the maxima or more simply from

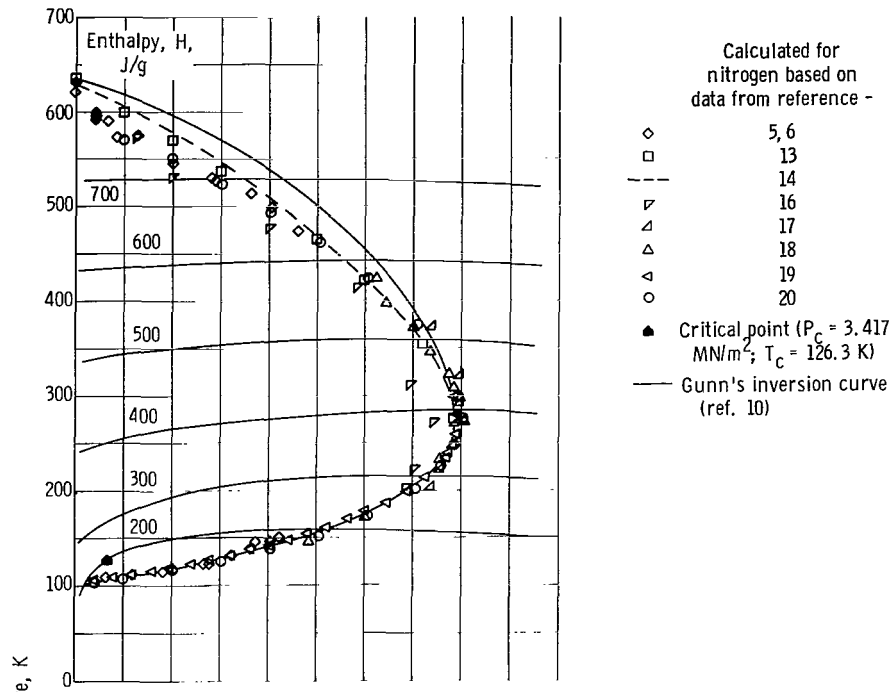
$$\frac{T}{\rho} \frac{\left(\frac{\partial P}{\partial T} \right)_\rho}{\left(\frac{\partial P}{\partial \rho} \right)_T} = 1 \quad (2)$$

A discussion of the relation between the isenthalpic and isothermal Joule-Thomson coefficients and their relation to the principle of corresponding states is found in appendix A. As pointed out in appendix A, the isenthalpic Joule-Thomson coefficient μ is not a corresponding states variable. However, the isothermal Joule-Thomson coefficient φ is a corresponding states variable. They are related by

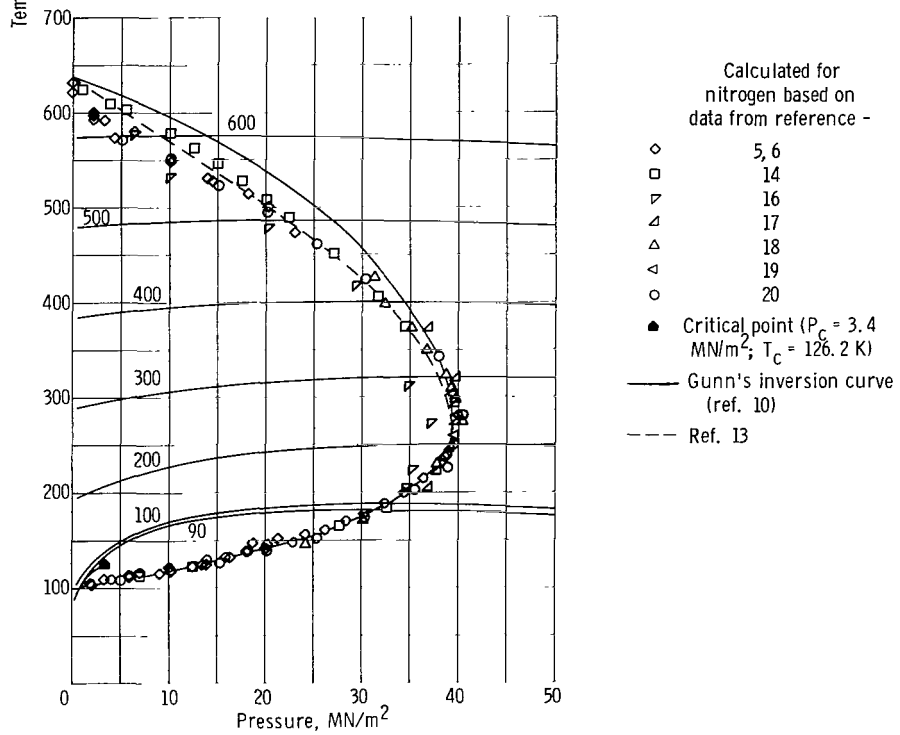
$$\varphi = -\mu C_p \quad (A3)$$

Now when $\varphi = 0$ $\mu = 0$ since $C_p \neq 0$; and consequently, the principle can be applied to the locus of points where $\mu = 0$.

The following discussion of inversion curves includes the nonreduced and reduced forms. Two fluids, nitrogen and oxygen, because they are well represented with reliable PVT data and J-T data in the literature, are treated in both forms. Reduced curves are presented for the eight fluids of reference 15 along with some preliminary results for hydrogen and some noble gases.



(a) Calculations based on PVT extensions of reference 14.



(b) Calculations based on reference 13.

Figure 6. - Joule-Thomson inversion curve for nitrogen. Curve and selected isenthalps calculated from reference 15; data are from references 5, 6, and 14 to 20.

Nonreduced Inversion Curves for Nitrogen and Oxygen

Nitrogen is a very useful research fluid and thus several sets of data for the inversion curve appear in the literature. The experimental Joule-Thomson inversion curve from the data of Roebuck and Osterberg (ref. 5), Deming and Shupe (refs. 16 and 17), Lunbeck, Michels, and Wolkers (ref. 18), Dean and Mann (ref. 19), and Din (ref. 20), along with the inversion curve calculated from the equation of reference 10, are plotted in figures 6(a) and (b). The inversion curve as calculated by using the Coleman-Stewart equation of state (ref. 13) is illustrated as a set of data points in figure 6(a) in order to distinguish it from the inversion curve calculated by using the extrapolated Bender equation of state (ref. 14), which is plotted as a dashed line. As can be seen, the agreement between the data and the calculated inversion curve is quite good, indicating that such calculations for other fluids should, in the absence of data, be reasonably good approximations. Also plotted are selected enthalpies to illustrate their general behavior in the P-T plane and in particular near the inversion and saturation curves.

In figure 6(b) the exercise of figure 6(a) is repeated by using the Coleman-Stewart equation of state (ref. 13) to generate the dashed line. As can be seen, the inversion curves are in good agreement, as are the selected isenthalps. This lends a great deal of confidence to the extrapolated PVT results.

Oxygen has significant applications in the nation's space program and in industrial usage. The recent PVT data of Weber (ref. 12) are very accurate, and a portion of the inversion curve was defined by Weber (ref. 12). The inversion curve calculated by using the extrapolated PVT results of Bender (ref. 14) and the data of Weber (ref. 12) are given in figure 7. As can be seen, the agreement is quite good; however, there is no verification of the high-temperature portion of the inversion curve. Again selected enthalpy values are overlaid on figure 7 to illustrate isenthalpic behavior for oxygen in the P-T plane.

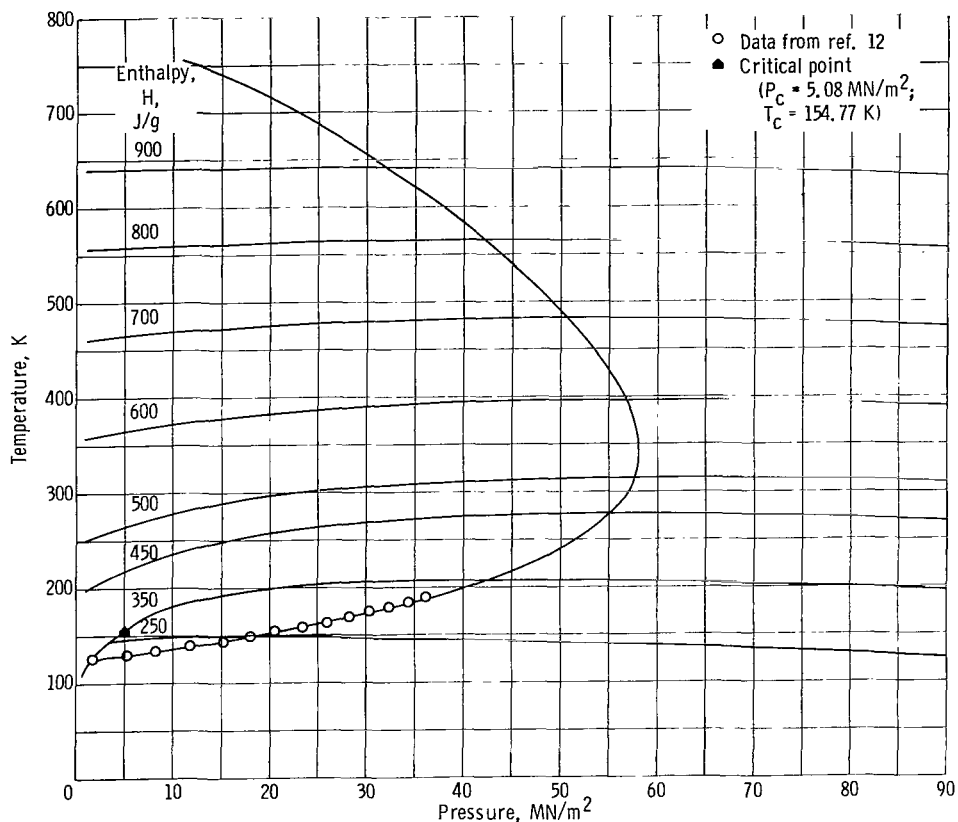


Figure 7. - Joule-Thomson inversion curve for oxygen. Curve and selected isenthalps based on PVT extensions as calculated from reference 15; data from reference 12.

Reduced Inversion Curves

In references 8 to 10, to cite a few, the principle of corresponding states was used to group the inversion curves. (See appendix A on the applicability of the principle.) Furthermore, Gunn, Chueh, and Prausnitz (ref. 10) found that several fluids (nitrogen, argon, xenon, carbon monoxide, methane, and ethylene) could be represented by a single inversion curve, while quantum fluids such as neon, hydrogen, and helium would not fit the pattern.

Since the principle of corresponding states should be applicable at high temperatures, Gunn, Chueh, and Prausnitz (ref. 10) force-fit the inversion data for hydrogen and helium to make their maximum inversion temperature coincide with that of the other fluids, and thereby defined pseudocritical values for the two fluids (refs. 10 and 21).

The inversion curves for methane, nitrogen, oxygen, argon, carbon dioxide, carbon monoxide, neon, nitrogen (Coleman and Stewart, ref. 13), and helium were calculated by using the extrapolated PVT results and plotted in reduced coordinates as figures 8 and 9. The inversion curve for hydrogen (fig. 9(c)) and portions of the inversion

Data from
reference -

- 5, 6
- △ 12
- ◇ 16
- ▽ 17
- 18
- ▽ 20
- ▽ 22
- ▲ Maximum inversion
temperature

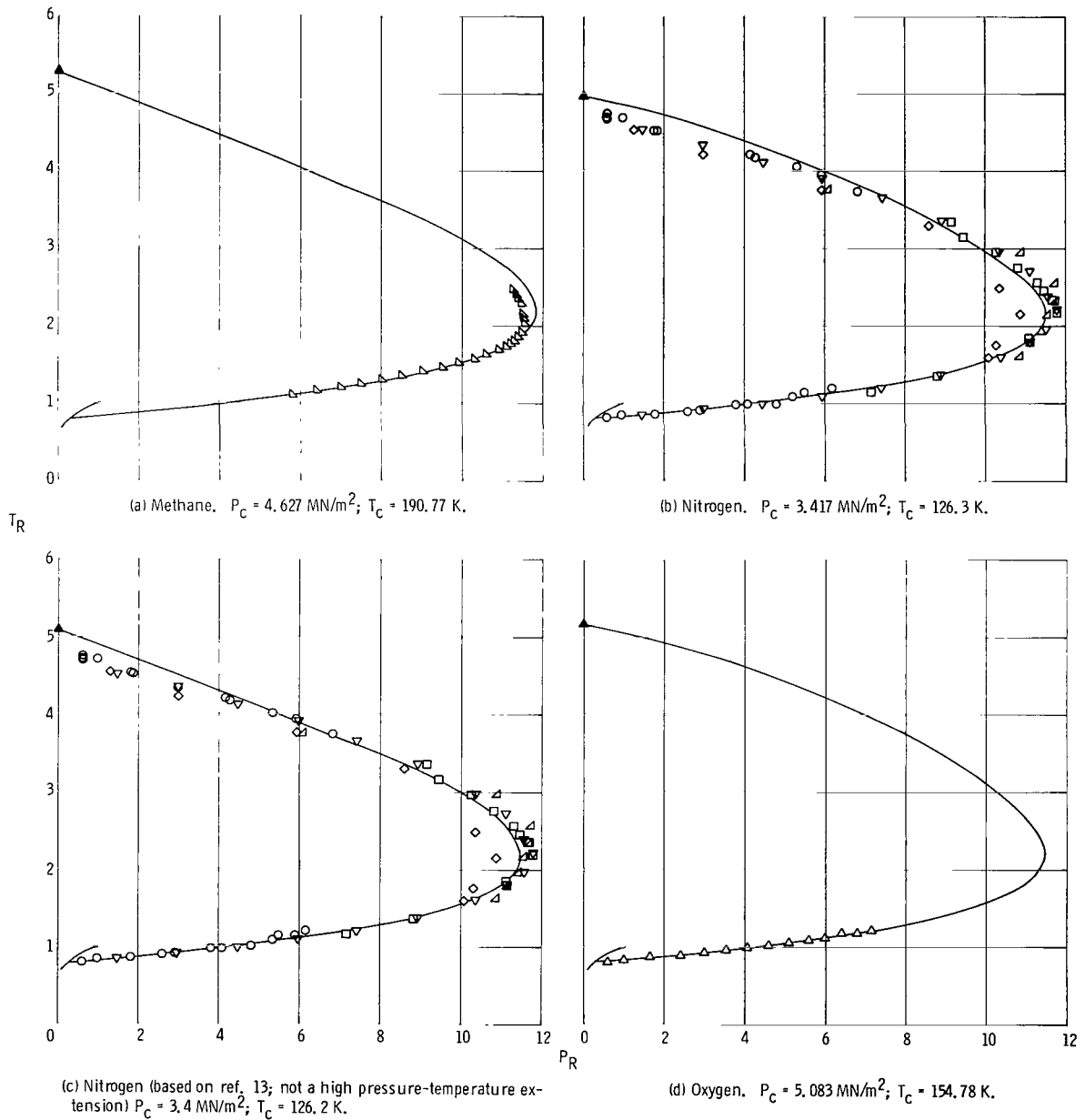
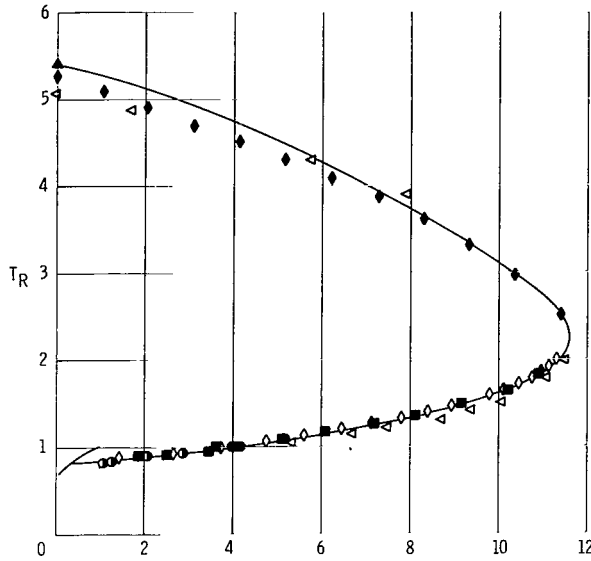
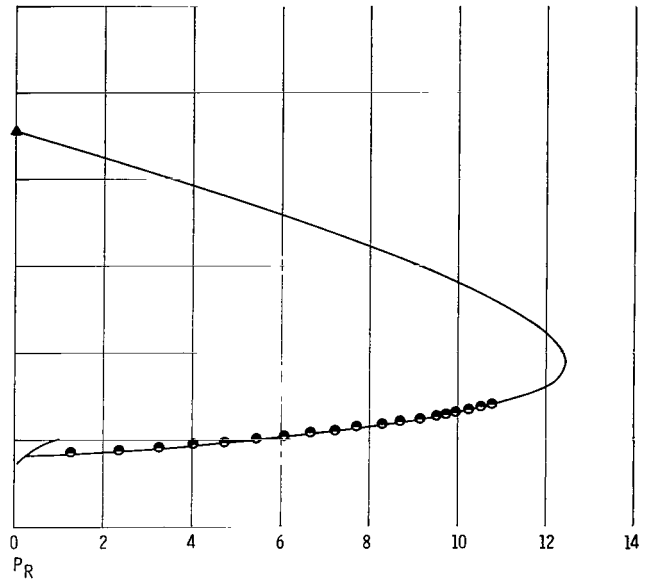


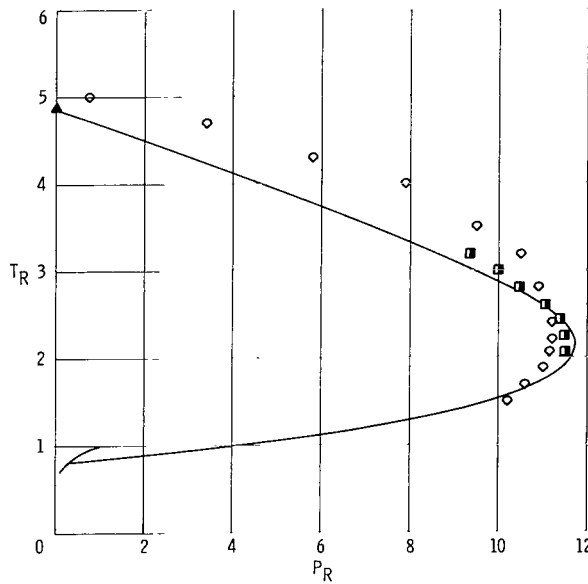
Figure 8. - Reduced Joule-Thomson inversion curve for several fluids, at various critical pressures P_C and critical temperatures T_C based on PVT extensions as calculated from reference 15. Available data included for comparison.



(e) Argon. $P_C = 4.865 \text{ MN/m}^2$; $T_C = 150.70 \text{ K}$.



(f) Carbon dioxide. $P_C = 7.3835 \text{ MN/m}^2$; $T_C = 304.21 \text{ K}$.



(g) Carbon monoxide. $P_C = 3.4986 \text{ MN/m}^2$; $T_C = 132.91 \text{ K}$.

- Data from reference -
- 4, 7
 - 27, 28
 - △ 10 (Kihara potential)
 - ◇ 23
 - ◆ 23 (extrapolated data)
 - 24 to 26
 - 30
 - ◇ 29
 - ▲ Maximum inversion temperature

Figure 8. - Concluded.

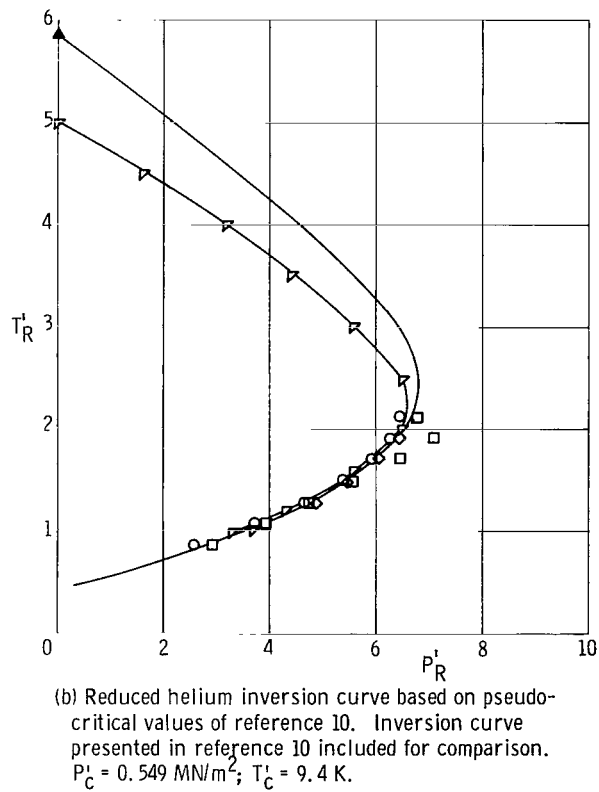
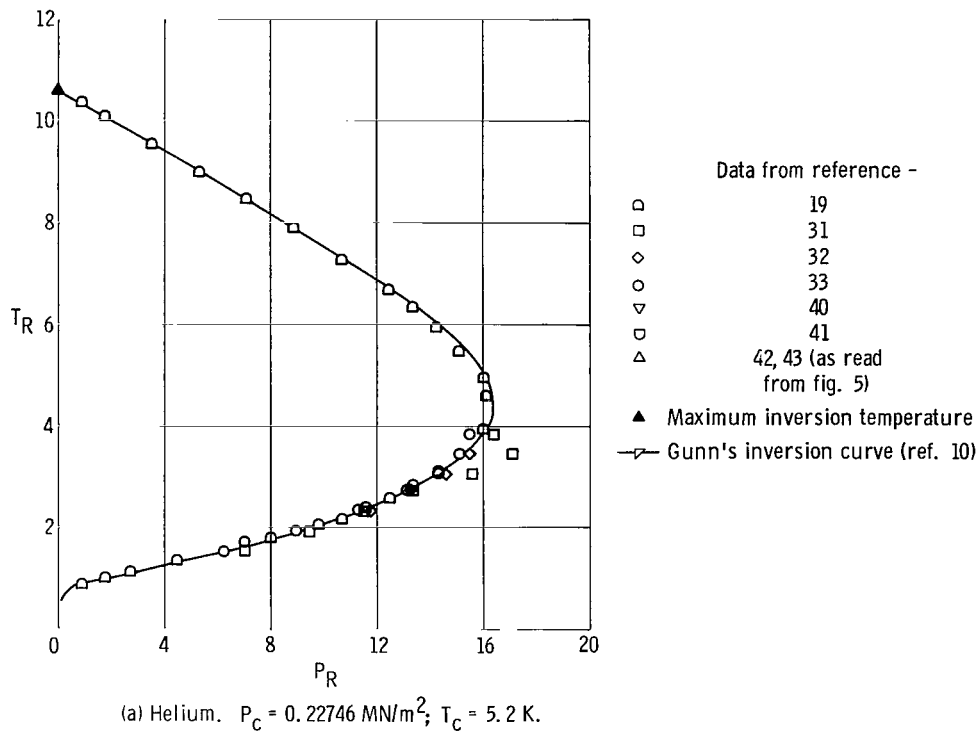
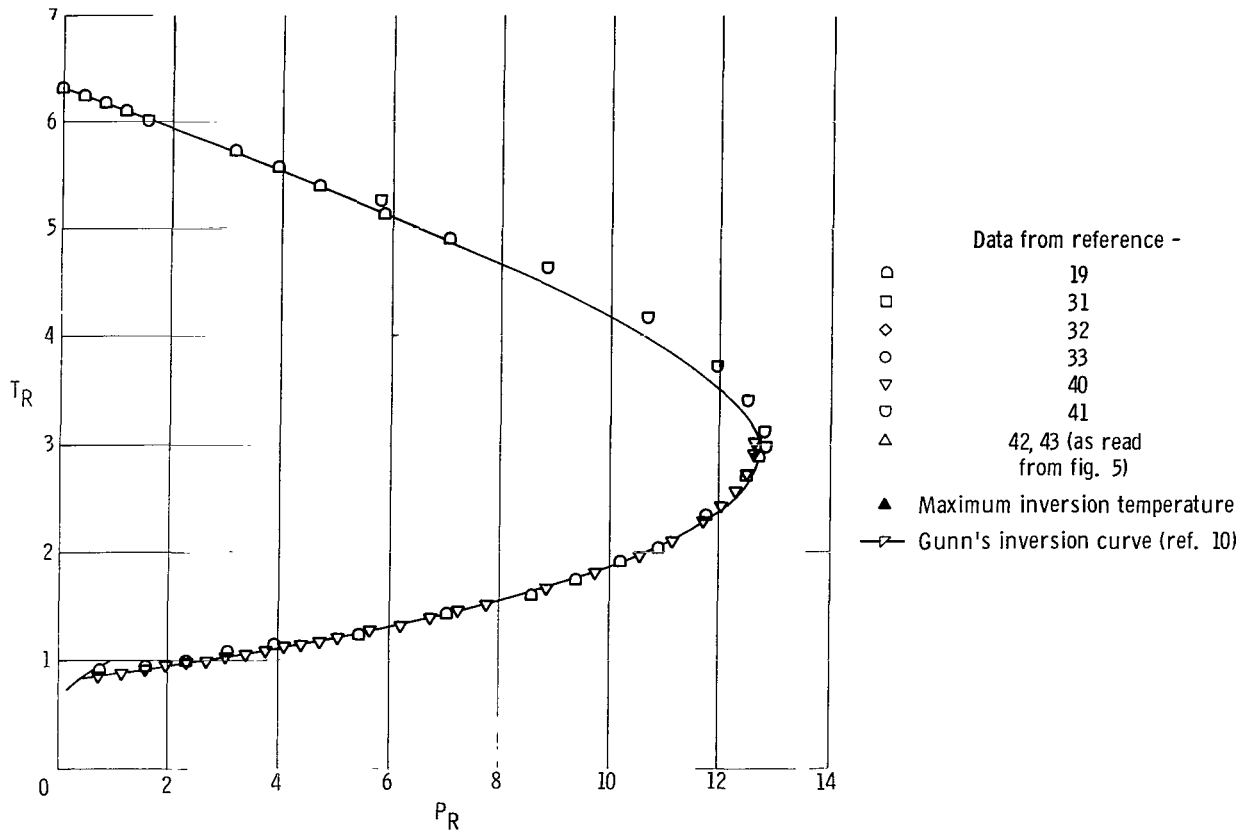
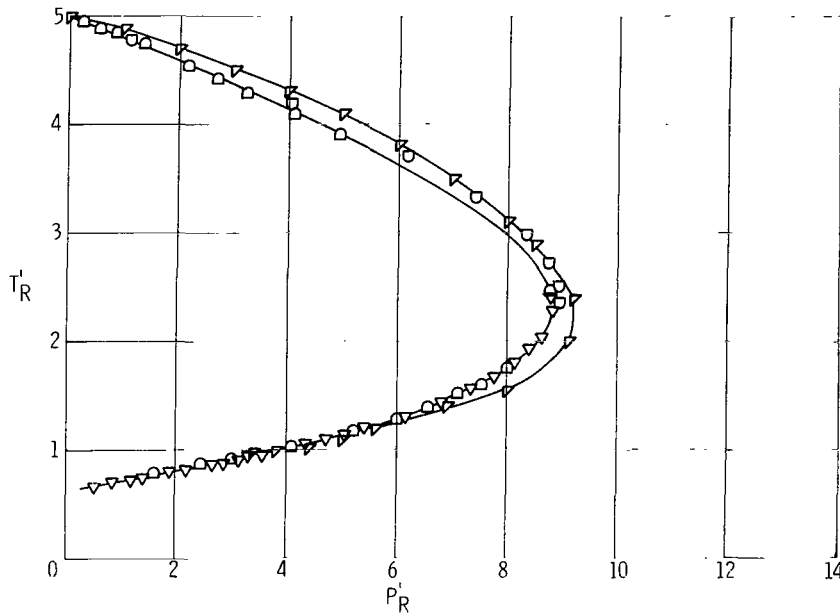


Figure 9. - Reduced Joule-Thomson inversion curves for the quantum fluids helium, hydrogen and neon, for various values of critical pressure P_c and critical temperature T_c .

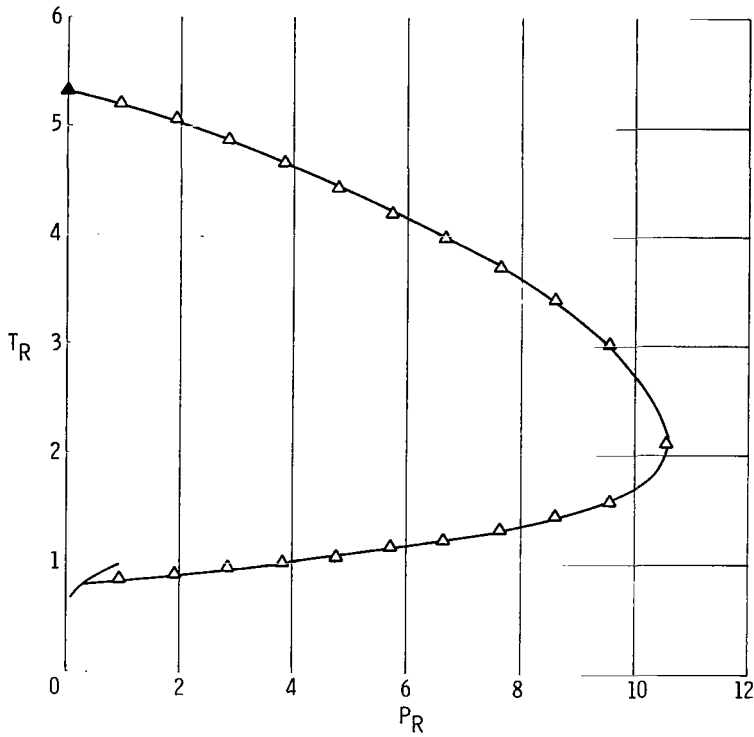


(c) Hydrogen. $P_C = 1.294 \text{ MN/m}^2$; $T_C = 32.984 \text{ K}$.

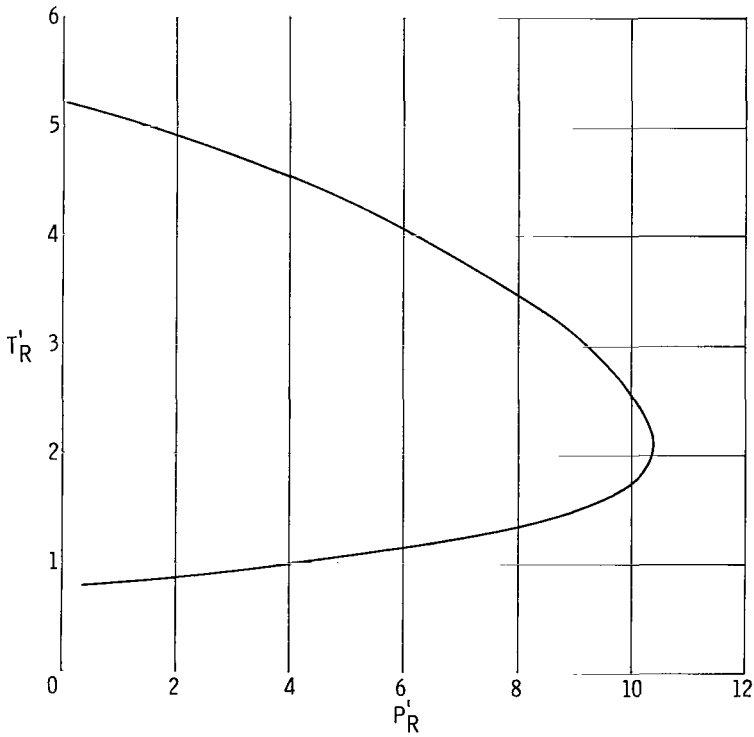


(d) Reduced hydrogen inversion curve based on pseudocritical values of reference 10. Inversion curve presented in reference 10 included for comparison. $P'_C = 1.854 \text{ MN/m}^2$; $T'_C = 41.4 \text{ K}$.

Figure 9. - Continued.



(e) Neon. $P_C = 2.6537 \text{ MN/m}^2$; $T_C = 44.40 \text{ K}$.



(f) Reduced neon inversion curve based on pseudocritical values of reference 10. $P'_C = 2.705 \text{ MN/m}^2$; $T'_C = 45.3 \text{ K}$.

Figure 9. - Concluded.

curves for xenon and krypton are presented (figs. 10 and 11). The helium, hydrogen, and neon² pseudoreduced plots as suggested by Gunn, Chueh, and Prausnitz (ref. 10) are also presented for comparison (figs. 9(b), (d), and (f)). The maximum inversion temperature (above which expansion produces heating at all pressures) as calculated in appendix B and summarized in table I is plotted on the inversion curve for each fluid. The Boyle temperature T_B and the low-density Joule inversion temperature $T_{B_{\max}}$ are also discussed in appendix B and tabulated in table I. However, for fluids considered herein, no calculated $T_{B_{\max}}$ was found. The behavior of these temperatures is relevant to the second virial coefficient B and its relation to the principle of corresponding states (see appendixes A and B).

Corresponding States Fluids

In figure 8(a) the inversion curve for methane is in good agreement with the limited methane data of Tester (ref. 22), except near the knee of the curve. As the isenthalps are extremely flat in this region, small errors in PVT and in the partial derivatives can result in large shifts in the inversion curve. As the PVT data used here are from reference 14, it is assumed that the inversion locus is more accurate than that of Tester (ref. 22).

In figures 8(b) to (d) the nitrogen and oxygen inversion curves and data are replotted in reduced coordinates. The agreement has been discussed previously.

In figure 8(e) the inversion curve for argon is plotted along with the data of Roebuck and Osterberg (refs. 4 and 7); Grossman, McCarty, and Hust (ref. 23); and Michels et al. (refs. 24 to 26); and the Kihara potential as calculated by Gunn (ref. 10). The agreement is quite good up to $T_R = 3$. From $T_R = 3$ to the maximum inversion temperature the relative error is at most 5 percent with respect to the results of reference 23. Since the calculated data points of reference 23 and the inversion curve of figure 8(e) are both based on an extrapolation of the equation of state, the deviations seem quite reasonable. As such, the relative error could be used as an indicator of the confidence which can be placed in the maximum inversion temperature.

In figure 8(f) the inversion curve for carbon dioxide is in good agreement with the data of Roebuck, Murrell, and Miller (ref. 27) and Newitt, Pai, Kuloor, and Huggill (ref. 28). Note that the shape of the reduced inversion curve deviates significantly from that of argon (fig. 8(e)). We also note that the acentric factor for argon is -0.002 and

²The quantum fluids, helium, hydrogen, and neon, are treated separately. Neon is considered a weak quantum fluid.

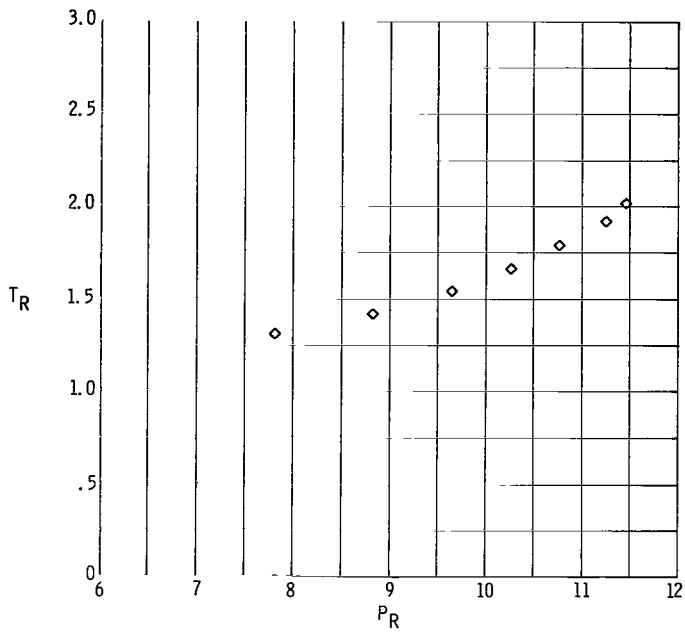


Figure 10. - Reduced Joule-Thomson inversion data for krypton from reference 44. Critical pressure, $P_c = 5.502 \text{ MN/m}^2$; critical temperature, $T_c = 209.4 \text{ K}$.

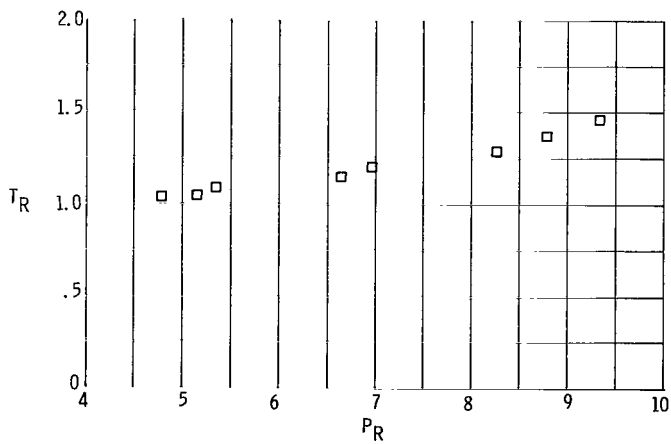


Figure 11. - Reduced Joule-Thomson inversion data for xenon from reference 45.

TABLE I. - FIXED-POINT TEMPERATURES RELATED TO
SECOND VIRIAL COEFFICIENT B

Fluid	Maximum inversion temperature (B/T = -maximum), T_{inv}	Low-density Joule inversion temperature (B = maximum), T_{Bmax}	Boyle temperature (B = 0), T_B	Reduced temperatures		
				$T_{R, inv}$	$T_{R, Bmax}$	$T_{R, B}$
CH ₄	1008.55	----	518.9	5.2867	----	2.72
^a N ₂	626.78	2140	321.4	4.9627	16.94	2.544
O ₂	798.98	----	403.3	5.162	----	2.606
Ar	815.06	----	412.7	5.4085	----	2.738
CO ₂	1387.78	----	725.8	4.5619	----	2.386
Ne	236.03	----	122.9	5.316	----	2.767
He	55.13	196	27.5	10.601	37.7	5.292
CO	647.51	----	347.9	4.872	----	2.618
^b N ₂	644.4	2140	329.8	5.102	16.94	2.61

^aFrom ref. 14.

^bFrom ref. 13.

TABLE II. - COMPARISON OF CRITICAL ISENTHALPIC JOULE-THOMSON COEFFICIENTS

AS CALCULATED FROM REFERENCE 15 AND $\mu_c = T_c/6P_c$

Fluid	Acentric factor (ref. 50), ω	Critical pressure, P_c		Critical temperature, T_c	Critical density, ρ_c , g/cm ³	Critical isenthalpic Joule-Thomson coefficient	
		atm	MN/m ²			$\mu_c = \frac{T_c}{6P_c}$, K/MN/m ²	$\mu_c = \left[\left(\frac{\partial P}{\partial T} \right)_{\rho} \right]^{-1}$ (from ref. 15)
CH ₄	+0.013	45.66	4.627	190.77	0.162	6.87	6.88
^a N ₂	+.04	33.72	3.417	126.3	.3105	6.16	5.91
O ₂	+.021	50.16	5.083	154.78	.4325	5.08	5.18
Ar	-.002	48.01	4.865	150.7	.531	5.16	5.58
CO ₂	+.42	72.87	7.3835	304.21	.464	6.87	5.56
Ne	0	26.19	2.6537	44.4	.483	2.79	4
CO	+.041	34.53	3.4986	132.91	.2997	6.33	3.96
He	0	2.245	.227464	5.2	.0693	3.81	7.9
^b N ₂	+.04	33.56	3.4	126.2	.3053	6.19	6.22
Xe	+.002	58	5.877	289.75	1.1052	8.22	----
Kr	-.002	54.3	5.502	209.4	.908	6.34	----
H ₂	0	12.77	1.294	32.984	.03077	4.248	----

^aFrom ref. 14.

^bFrom ref. 13.

that for carbon dioxide is 0.42 (table II and appendix C), which means that carbon dioxide deviates considerably from the principle of corresponding states.

In figure 8(g) the inversion curve for carbon monoxide departs significantly from the data of Leah (ref. 29); however, the departure is not quite so significant for the data of Michels, Lunbeck, and Wolkers (ref. 30). The most troublesome aspect of these extrapolated results is the significant departure from the general form of the inversion curve for other corresponding states fluids. The results of Leah (ref. 29) and those of reference 15 were compared in depth, and are discussed in appendix E. There do seem to be systematic deviations in the results of Leah (ref. 29) and those of reference 15; however, the deviations persist into the regime where reference 15 is more accurate than reference 29. Thus, the inversion curve is questionable at high temperatures. The corresponding states form is definitely favored.

Quantum Fluids

Helium, hydrogen, and neon are quantum fluids and, as such, depart from a corresponding states treatment. However, neon appears to behave more like a normal fluid and is usually considered to be a weak quantum fluid.

The inversion curve for helium and the data of Baehr (ref. 31), Keesom (ref. 32), and Hill and Lounasmaa (ref. 33) are plotted in figures 9(a) and (b). In general, the data are in good agreement with the curve; however, one data point of Baehr (ref. 31) seems to be out of line. The maximum inversion temperature of helium has been calculated by several researchers: Beattie (ref. 34) and Keyes (ref. 35), 45 K; Kirkwood and Keyes (ref. 36), 54 K; Roebuck (refs. 2 and 3) estimated 23.6 K by using the reduced temperature of 4.55 K for air; Gunn, Chueh, and Prausnitz (ref. 10), 47.7 K; and an observed value of 34 K as listed by Crawford (ref. 37). Dean and Mann (ref. 19) use 55 K in their analysis of the Joule-Thomson refrigerator. The maximum inversion temperature of table II (appendix C) is 55 K. The agreement of the curve with reference 19 is not surprising as the equation of state used in reference 15 is that of Mann (ref. 38). The reduced inversion curve for helium (fig. 9(b)) is based on the pseudocritical parameters $T_c = 9.4$ K and $P_c = 0.5492$ MN/m² as suggested by Gunn, Chueh, and Prausnitz (ref. 10). Superimposed on this figure is the helium inversion curve determined in reference 10 for comparison.³ Generally, the discrepancies are large on the upper part of the inversion curve, as would be expected from the lack of agreement in the maximum

³Gunn, Chueh, and Prausnitz (ref. 10) developed three distinct curves: one for helium, one for hydrogen, and one for the corresponding states fluids.

inversion temperature, 47.7 K (ref. 10) to 55 K (appendix A and table I). This would mean that the pseudocritical temperature would have to be 10.8 K in order to force agreement with the general reduced inversion temperature of 5.095 K (ref. 10).

In figure 9(c), the inversion curve for hydrogen was determined by using the program of Goldberg and Haferd (ref. 39), which is based on the PVT fit of Roder, Weber, and Goodwin (ref. 40). The data of Michels, DeGraaf, and Wolkers (ref. 41) are generally in good agreement with the curve; however, they appear high. The lower temperature data of reference 40 are in good agreement, as would be expected. In figure 9(d), the reduced hydrogen inversion curve is based on the pseudocritical values of reference 10, $T_c = 41.4$ K and $P_c = 1.854$ MN/m². As might be expected, the agreement between the curves of Gunn, Chueh, and Prausnitz (ref. 10) and the inversion curves is quite good as they came from the equivalent data sets.

In figure 9(e) the reduced inversion curve for neon agrees very well with the smoothed data of McCarty and Stewart (ref. 42) and Michels and Gibson (ref. 43). This is not too surprising since the maximum inversion temperature was used as a constraint in determining the equation of state (ref. 42). In figure 9(f) the reduced neon curve is based on the pseudocritical values $T_c = 45.3$ K and $P_c = 2.705$ MN/m² (ref. 10). In comparing the curves (figs. 9(e) and (f)) there appears to be little difference between them. (Recall that neon is considered a weak quantum fluid.)

Other Joule-Thomson Data

The data of Trappeniers, Wassenaar, and Wolkers (ref. 44) and Michels, Wassenaar, DeGraaf, and Wolkers (ref. 45) were used to obtain portions of an inversion curve for krypton and xenon, respectively (figs. 10 and 11). The general trends of the data appear to be in good agreement with other fluids and are included in order to form a more general reduced inversion curve applicable to several fluids, as discussed later.

Equations for Inversion Curves

The reduced inversion curves for methane, nitrogen, oxygen, carbon dioxide, carbon monoxide, argon, neon, helium, and hydrogen have been fitted by using a least-squares technique from $T_R \approx 0.9$ ($P_R \approx 2$) to the maximum inversion temperature with a polynomial

$$P_R = \sum_{i=0}^6 A_i T_R^i$$

TABLE III. - POLYNOMIAL COEFFICIENTS OF REDUCED INVERSION CURVES OF SEVERAL FLUIDS

$$\left[P_R = \sum_{i=0}^6 A_i T_R^i \right]$$

Fluid	Number of points used in each fit, n	A ₀	A ₁	A ₂	A ₃	A ₄	A ₅	A ₆	Average sums of square of residuals, E _r ×100
Methane	28	-31.2651873	60.3026109	-32.9452939	9.29996645	-1.50083567	0.12645882	-0.0041500129	0.59
^a Nitrogen	37	-32.2267981	64.2512980	-37.7834487	11.966361	-2.29966244	.25510747	-.012830057	.58
^b Nitrogen	22	-35.7879152	72.8486137	-45.6317248	15.2554526	-2.90682623	.28560901	-.010865648	1.1
Oxygen	34	-36.2893677	75.0939713	-48.741621	17.2310336	-3.57529548	.40633931	-.01973906	.77
Argon	30	-25.2735214	47.0015602	-22.2479188	5.10306394	-.67161214	.054807958	-.0025724488	.31
Carbon dioxide	26	-49.6820235	106.352075	-72.1171474	25.3427205	-5.00402093	.51606354	-.021543775	.9
Neon	30	-41.3301625	86.5178852	-59.0821381	21.5253196	-4.46121949	.49273197	-.02267271	7.6
Carbon monoxide	32	-24.5141408	44.1764731	-18.5476859	3.23409545	-.26868672	.014909515	-.001050672	1.5
Hydrogen	21	-15.5988252	26.0321395	-9.7459013	2.4207304	-.49105816	.05932495	.002913248	.18
Helium	26	-9.50023901	13.4661013	-2.1997754	.14814825	-.01540754	.00173746	-.7093585×10 ⁻⁴	1.1
General ^c		β ₀	β ₁	β ₂	β ₃	β ₄	β ₅	β ₆	
		-32.5209374	65.6922312	-39.7384300	12.9300299	-2.46176904	0.25378553	-0.010986565	

^aFrom ref. 14.

^bFrom ref. 13.

^cFor fluids with small acentric factors. Helium, hydrogen, and neon are not included due to quantum effects.

The coefficients for these fluids are given in table III, along with the average sums of the squares of the residuals

$$E_r = \frac{1}{n} \sum (P_R - P_{R, \text{data}})^2$$

Generalized Reduced Inversion Curve

In forming a generalized reduced inversion curve, inversion data for the fluids argon, methane, oxygen, and nitrogen and the data for fluorine (ref. 46), xenon, and krypton were weighted equivalent. The carbon monoxide data of Leah (ref. 29) and Michels, Lunbeck, and Wolkers (ref. 30) and points from the inversion locus of figure 8(g) were weighted equivalent but not used in the fit; however, they are centered about the general inversion curve. The fluids helium, hydrogen, and neon were not used because of the quantum effects cited previously. Carbon dioxide was not used because of its large acentric factor (0.42, table II and appendix C). Within these restraints, and recalling that much of the curves were calculated from extrapolated PVT data as discussed previously, the locus of points in figure 12 is a least-squares representation of all the data for the corresponding states fluids. The generalized inversion curve is described by

$$P_R = \sum_{i=0}^6 \beta_i T_R^i$$

The coefficients β_i are tabulated in table III. The agreement between the general reduced inversion curve presented herein and that of Gunn, Chueh, and Prausnitz (ref. 10) is quite good for $T_R < 3$, as can be seen from figure 12.

Although the quantum fluids and their isotopes should be handled separately (e.g., refs. 10 and 21), the reduced inversion curves could probably be brought together by finding (empirically) the suitable pseudocritical temperature and pressure for each fluid. Figure 13 illustrates the pseudoreduced inversion curves for the quantum fluids relative to the generalized reduced inversion curve of figure 12.

- Methane (ref. 22)
- ▽ Argon (refs. 4, 7, 10, 23 to 26)
- Oxygen (ref. 12)
- ◇ Carbon monoxide (fig. 8(g))
- Nitrogen (refs. 5, 16 to 18, and 20)
- ▷ Krypton (ref. 44)
- ◁ Xenon (ref. 45)
- Carbon monoxide (ref. 30)
- △ Carbon monoxide (ref. 29)
- ▷ Fluorine (ref. 46)
- Gunn's inversion curve (ref. 10)
- General inversion curve (this report)

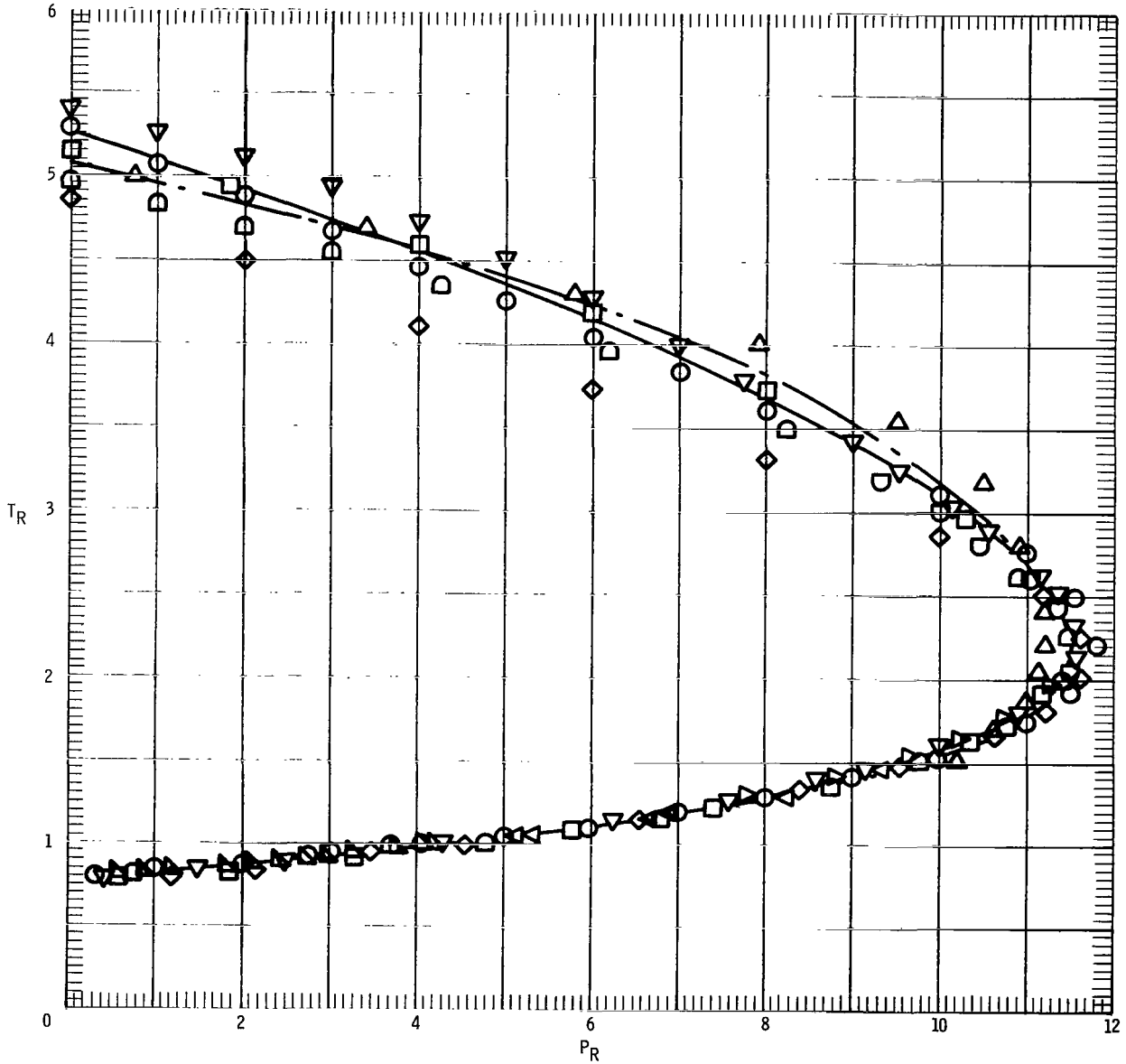


Figure 12. - Generalized reduced Joule-Thomson inversion curve for several corresponding states fluids, based on the PVT extensions and data. Curve of reference 10 included for comparison.

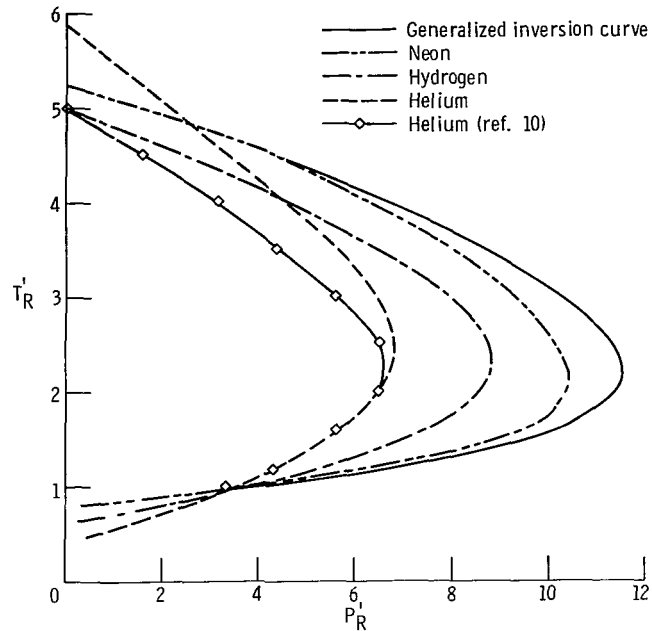


Figure 13. - Generalized reduced Joule-Thomson inversion curve of figure 12 and pseudoreduced inversion curves of quantum fluids helium, hydrogen, and neon. Inversion curve for helium of reference 10 included for comparison. (For nonquantum fluids, $T'_R = T_R$ and $P'_R = P_R$.)

Joule-Thomson Coefficients

With the aid of a computer program (e. g., ref. 15), the isenthalpic Joule-Thomson coefficients (eq. (1)) can be calculated over a wide range of temperatures and pressures. Curves of μ against T with P as a parameter, T against P with μ as a parameter, or various combinations can be fabricated.

Reduced Joule-Thomson Coefficients

In appendix C, a technique for determining the Joule-Thomson coefficient at the critical point is discussed

$$\mu_c^{-1} = \left(\frac{\partial P}{\partial T} \right)_{\rho} \Big|_c \quad (C4)$$

or, in normalized form, in terms of the dimensionless parameter,

$$\frac{T_c}{P_c \mu_c} = \left[\left(\frac{\partial \ln P}{\partial \ln T} \right)_{\rho} \right]_c \quad (C5)$$

The difficulty is, of course, obtaining a proper derivative in the critical region; and based on the work of Bender (ref. 14), Coleman and Stewart (ref. 13), and reference 15, the normalized dimensionless parameter $T_c/P_c \mu_c$ is nearly a constant. Thus, a simplified form of μ_c is proposed

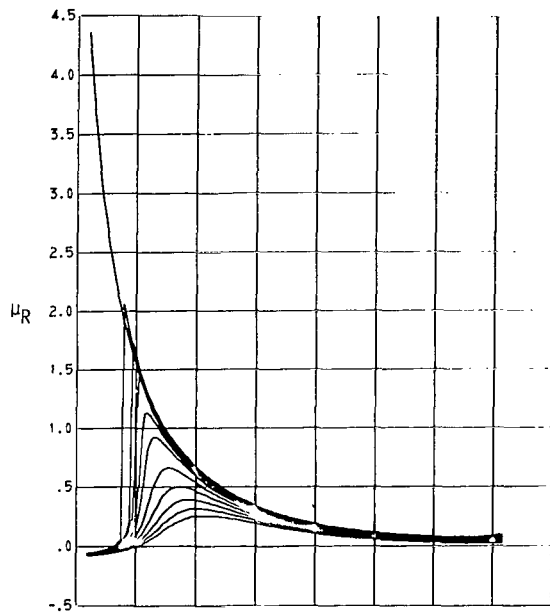
$$\mu_c \approx \frac{T_c}{6P_c} \quad (C7)$$

For the fluids discussed herein, the values of μ_c are tabulated (table II and appendix C). As can be seen the values are quite reliable except for helium, neon, and carbon monoxide. The equations of state for these fluids were fit many years ago and should probably be reexamined in the critical region. It must be pointed out that the values of μ_c for nitrogen as calculated by reference 15 from the state equations of Coleman and Stewart (ref. 13) and Bender (ref. 14) are 6.22 and 5.91, respectively. Moreover, Roebuck and Osterberg (ref. 5) experimentally determined $(\mu_c)_{N_2} = 5.72$. The agreement with equation (C6) $\left[(\mu_c)_{N_2} = 6.17 \right]$ is quite good when the difficulties in calculating $\left[(\partial P / \partial T)_{\rho} \right]_c$ are considered.

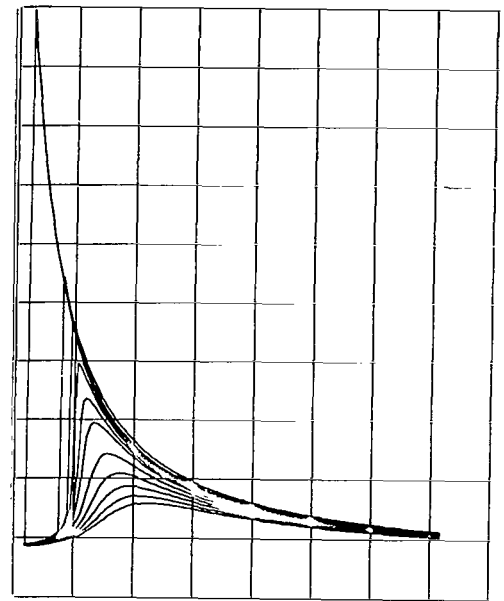
By using $\mu_c = T_c/6P_c$, reduced Joule-Thomson coefficients ($\mu_R = \mu/\mu_c$) as functions of reduced temperature T_R with reduced pressure P_R as the parameter are presented in figure 14 for methane, nitrogen (ref. 14), oxygen, argon, carbon dioxide, carbon monoxide, neon, and nitrogen (ref. 13).

Constant Joule-Thomson Loci

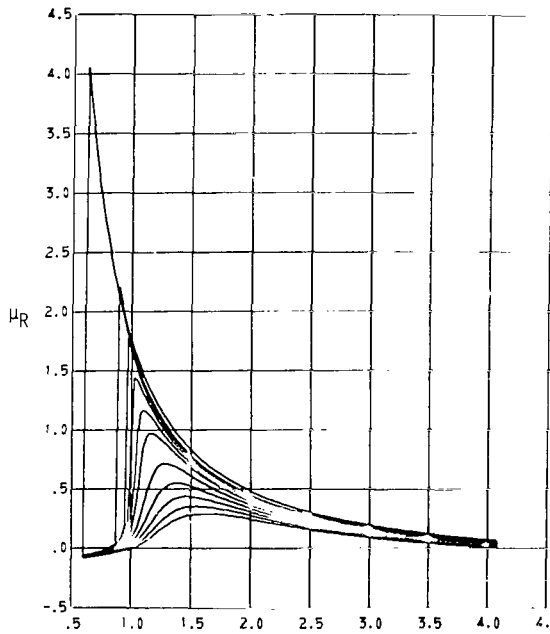
Interpolating the μ - T figure with P as the parameter, curves of constant μ can be plotted as a function of temperature and pressure. The calculated values from the state equations of references 13 and 14 in reference 15 for nitrogen for constant μ are compared with the data of Roebuck and Osterberg (ref. 5) in figure 15. As can be seen, the calculated values are in good agreement; however, there is some disagreement in the $\mu < 0$ regime between the calculated values and data of reference 5.



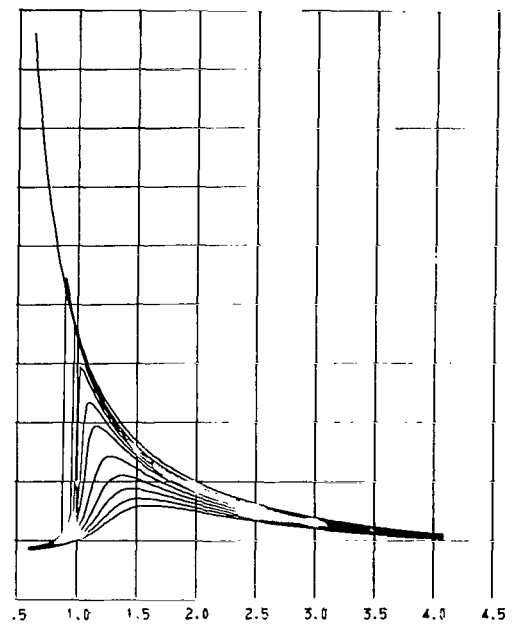
(a) Methane.



(b) Nitrogen (based on ref. 14).



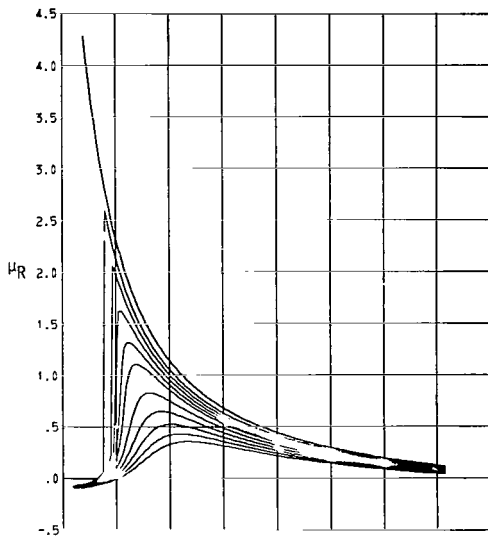
(c) Nitrogen (based on ref. 13).



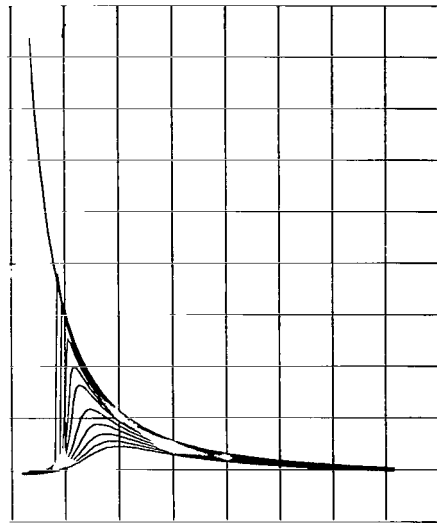
(d) Oxygen.

T_R (for $P_R = 0.5, 0.75, 1.0, 1.25, 1.5, 2.5,$ and 4.0 and $P = 1$ atm)

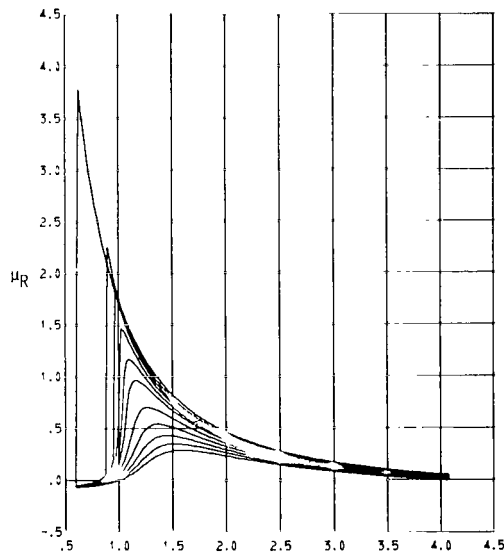
Figure 14. - Reduced Joule-Thomson coefficients as function of reduced temperature for selected isobars.



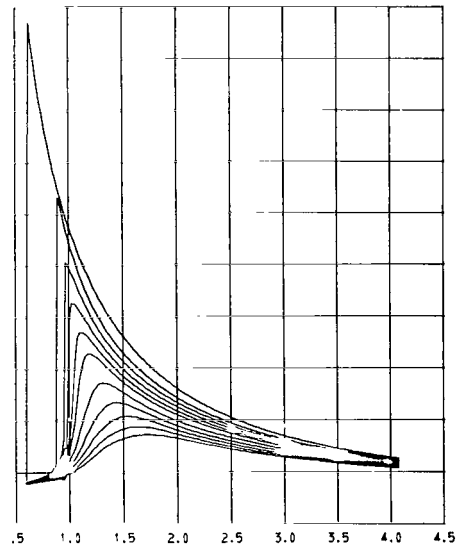
(e) Argon.



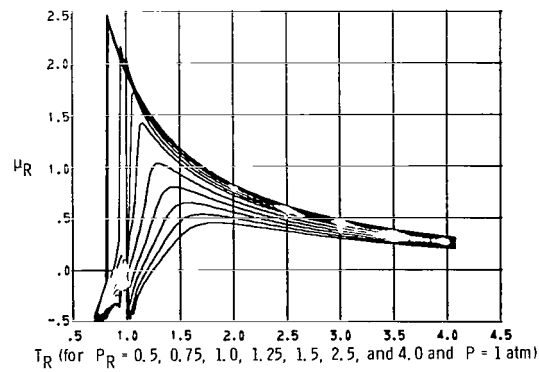
(f) Carbon dioxide.



(g) Carbon monoxide.



(h) Neon.



(i) Helium.
 T_R (for $P_R = 0.5, 0.75, 1.0, 1.25, 1.5, 2.5, \text{ and } 4.0$ and $P = 1 \text{ atm}$)

(i) Helium.

Figure 14. - Concluded.

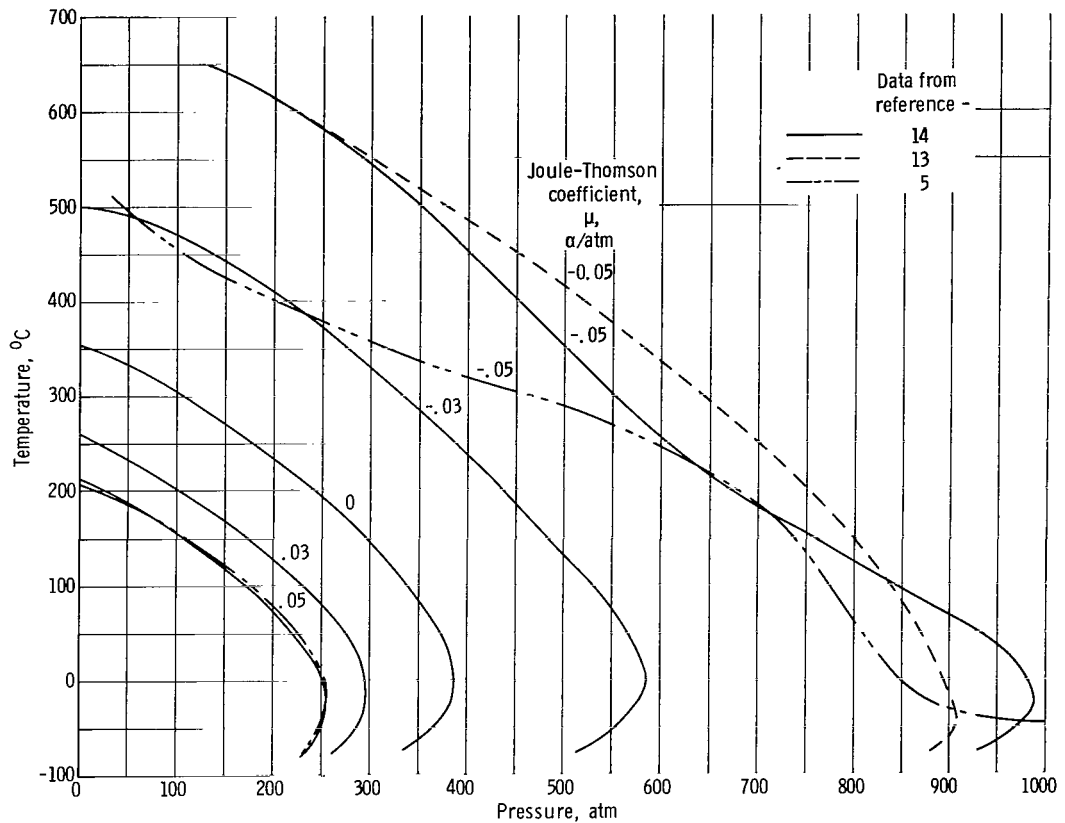


Figure 15. - Joule-Thomson coefficient contours based references 13 and 14, calculated from reference 15, as compared to the contours presented in reference 5.

Joule-Thomson Refrigerators and Liquifiers

Joule-Thomson refrigerators and liquifiers usually operate in the lowest temperature portion of the cycle. The thermodynamics and operating optimums are discussed in appendix D. It was determined that the governing equations for the optimum figure of merit (compressor power input/refrigeration output) for both the refrigerator and the liquifier were of the same form. Further, if the amount of gas liquified were zero, the governing equations for the refrigerator and liquifier were identical. Dean and Mann (ref. 19) solved the governing equations for helium, hydrogen, and nitrogen. Their results and those herein point out that maximum refrigeration (liquification) does not correspond to the maximum figure of merit, that is, optimum operating costs.

A qualitative look at the Linde intermediate pressure cycle reveals that the optimization procedure can only serve as a guide to the experiment. For example, the analysis tends to indicate that the intermediate pressure should be near P_c with $\dot{n}_2/\dot{m} >$

0.15. In the Linde process for liquifying air, the intermediate pressure is 40 atmospheres and $\dot{n}_2/\dot{m} = 0.2$ (ref. 47).

The operating costs can also be reduced by precooling the inlet gas and/or cascading using several single J-T cycles with different operating fluids.

CONCLUSIONS

The pressure-volume-temperature (PVT) relations for several fluids (methane, nitrogen, oxygen, argon, carbon dioxide, neon, carbon monoxide, fluorine, hydrogen, and helium) have been used to study the behavior of the isenthalpic and isothermal Joule-Thomson coefficients and in particular the inversion curve. The following conclusions were reached:

1. Examination of the PVT data obtained by extrapolating the equation of state described by Hendricks, Baron, Peller, and Pew indicates valid results for the high-pressure and high-temperature ranges. This is further validated by the fact that the partials $(\partial P/\partial \rho)_T$ and $(\partial P/\partial T)_\rho$, where ρ is density, are in good agreement with other high-pressure and -temperature results of Coleman and Stewart. The Joule-Thomson inversion curves calculated as functions of these extrapolated PVT data agree well with best available J-T data.

2. Since the Joule-Thomson inversion curve (isenthalpic J-T coefficient $\mu = 0$) conforms to the principle of corresponding states, a generalized, reduced inversion curve can be determined for the fluids with low acentric factors. Although the individual fit of the inversion curve for each fluid gives better results, the generalized curve is useful in the absence of data and to indicate similarities among the fluids. The inversion curve developed herein and that presented by Gunn, Chueh, and Prausnitz are in good agreement. The quantum fluids helium, hydrogen, and neon are best handled separately.

3. A critical isenthalpic Joule-Thomson coefficient μ_c can be determined and a simplified expression deduced for it:

$$\mu_c^{-1} = \left(\frac{\partial P}{\partial T} \right)_\rho \approx \frac{6P_c}{T_c}$$

Even though the corresponding states principle does not apply to $\mu \neq 0$, reduced curves can be determined and are useful in grouping data and where data are not available.

4. The maximum inversion temperature (maximum (B/T)) and the Boyle temperature ($B = 0$) can be found from the second virial coefficient B of the state equations. For the fluids with inversion curves calculated herein, no maximum in B was found.

5. Joule-Thomson liquifiers and refrigerators operate most efficiently at pressures substantially less than those corresponding to the maximum cooling capacity.

Lewis Research Center,
National Aeronautics and Space Administration,
Cleveland, Ohio, March 10, 1972,
113-31.

APPENDIX A

PRINCIPLE OF CORRESPONDING STATES AND THE INVERSION CURVE

The corresponding states principle applies to molecules with spherical symmetry and a universal curve shape for the potential energy of molecular interaction. Consequently, the principle applies only to those properties which depend on the intermolecular energy. As such, the reduced second virial coefficient $B\rho_c$ should be a universal function of reduced temperature T_R . Simple substances such as the inert gases (excluding helium, hydrogen, and possibly neon due to quantum effects), nitrogen, oxygen, carbon monoxide, and methane do conform as expected.

The second virial coefficient, to which the principle applies, is simply related to the isothermal Joule-Thomson coefficient

$$\varphi = \left(\frac{\partial H}{\partial P} \right)_T \quad (A1)$$

in the limit of zero pressure

$$\varphi_0 = \lim_{P \rightarrow 0} \varphi = \frac{B}{T} \left(T - \frac{d \ln B}{d \ln T} \right) \quad (A2)$$

Consequently, the principle of corresponding states is applicable to φ . Now φ is related to the isenthalpic Joule-Thomson coefficient μ by

$$\varphi = \left(\frac{\partial H}{\partial P} \right)_T = -C_p \left(\frac{\partial T}{\partial P} \right)_H = -\mu C_p \quad (A3)$$

Francis and Luckhurst (ref. 48) note that the principle of corresponding states in the low-pressure limit is not applicable to specific heat C_p or to the isenthalpic Joule-Thomson coefficient μ , even though their product is a corresponding states variable.

However, the application of the principle of corresponding states to the inversion curve, for the fluids indicated previously, is valid. The inversion curve represents the locus of points where

$$\mu C_p = 0 = \frac{1}{\rho} \left[\frac{T}{\rho} \frac{\left(\frac{\partial P}{\partial T} \right)_\rho}{\left(\frac{\partial P}{\partial \rho} \right)_T} - 1 \right] = -\varphi \quad (A4)$$

This, of course, also means that isothermal Joule-Thomson expansions for $\varphi < 0$ produce cooling and isothermal expansions where $\varphi > 0$ produce heating. However, the inversion curve, common to both isothermal and isenthalpic expansions, represents a locus of minimums of the isotherms in the enthalpy-pressure plane (fig. 16).

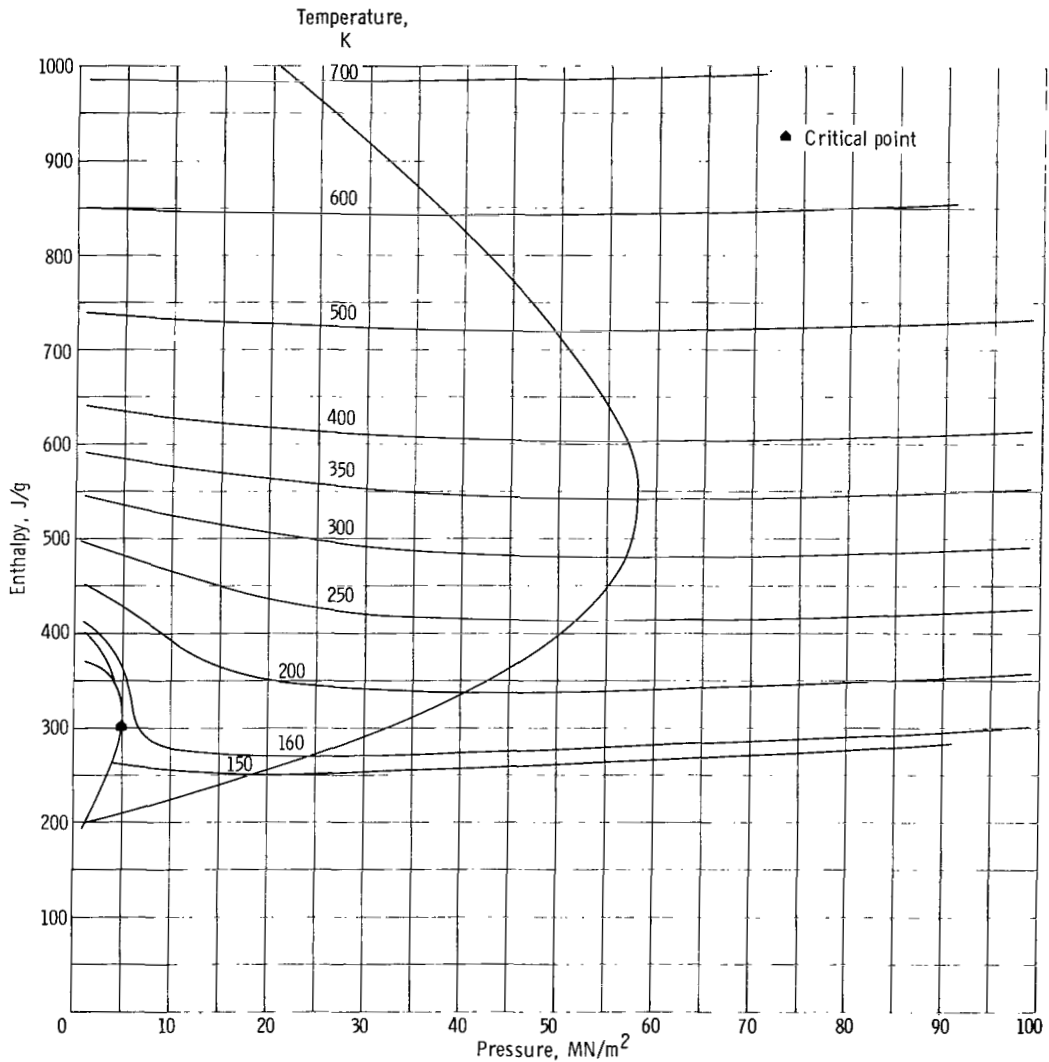


Figure 16. - Isothermal Joule-Thomson expansion ($\varphi = (\partial H / \partial P)_T = -\mu C_p$) and the inversion curve ($\varphi = -\mu C_p = 0$) for fluid oxygen.

APPENDIX B

INVERSION TEMPERATURES AND THE SECOND VIRIAL COEFFICIENT

The isothermal and isenthalpic Joule-Thomson coefficients, as discussed in appendix A, have been used to test virial forms of the equation of state and derived properties.

From reference 15 the equation of state can be written as

$$P = \rho RT + A(T)\rho^2 + B(T)\rho^3 + C(T)\rho^4 + D(T)\rho^5 + H(T)\rho^6 + [E(T) + F(T)\rho^2 + G(T)\rho^4]\rho^3 e^{(-n_20\rho^2/T_2)} \quad (B1)$$

where the functions $H(T)$ and $G(T)$ were added to accommodate Coleman and Stewart's equation for nitrogen (ref. 13). Expanding the exponential in a Taylor series about $\rho = 0$ and rearranging, the equation of state can be written as

$$\begin{aligned} \frac{P}{\rho RT} = Z = 1 + \frac{A(T)}{RT} \rho + \frac{B(T) + E(T)}{RT} e^{(-n_20\rho^2/T_2)} \rho^2 + \frac{C(T)}{RT} \rho^3 + \dots \\ = 1 + B\rho + C\rho^2 + D\rho^3 + \dots \end{aligned} \quad (B2)$$

where the first term represents a fluid with negligible molecular interaction (i.e., ideal gas). The second B , third C , or fourth D , etc., terms or virial coefficients represent interactions between two, three, or four molecules, etc., respectively. As such the virials B , C , D , etc., represent the deviation from an ideal gas state. Here we are interested in the second virial coefficient $B = A(T)/RT$, or from reference 15 with the modifications cited,

$$B = \frac{1}{R} \left(n_1 + \frac{n_2}{T} + \frac{n_3}{T^2} + \frac{n_4}{T^3} + \frac{n_5}{T^4} + \frac{n_{21}}{T^5} + \frac{n_{25}}{T^7} \right) \quad (B3)$$

The zero-pressure inversion temperature (maximum inversion temperature) is given in terms of the second virial coefficient for the equation of state

$$PV = RT \left(1 + \frac{B}{V} + \frac{C}{V^2} + \dots \right) = 1 + B'P + C'P^2 + \dots \quad (B4)$$

by the zero-pressure limit of φ (appendix A). Using equations (B1) and (1) we find the limit

$$\lim_{P \rightarrow 0} (-\varphi) = \lim_{P \rightarrow 0} \mu C_p = T^2 \frac{d(B/T)}{dT} \quad (\text{B5})$$

Since $C_p > 0$, μ passes through zero at the temperature for which B/T is a maximum. By using the second virial coefficient of reference 15 (eq. (B3)) and maximizing B/T , the zero-pressure inversion temperatures T_{inv} estimated by extrapolating the PVT results to higher temperatures are presented in table I. For the Van der Waal equation of state

$$P = \frac{RT}{V - b} - \frac{a}{V^2} \quad (\text{B6})$$

the second virial coefficient becomes

$$B = b - \frac{a}{RT} \quad (\text{B7})$$

and substituting equation (B7) into equation (B5) the maximum inversion temperature becomes

$$T_{\text{inv}} = \frac{2a}{Rb} \quad (\text{B8})$$

or in reduced form

$$T_{R, \text{inv}} = \frac{27}{4} \quad (\text{B9})$$

since Van der Waal's value of T_c is $8a/27Rb$. Meissner in the Handbuch der Physik (1926) found $T_{R, \text{inv}}$ to be about 5.8 for all gases, which is 14 percent lower than given by equation (B9) except, of course, for helium. However, the values presented in table I are even lower but are generally in good agreement with the results of Gunn, Chueh, and Prausnitz (ref. 10), where $T_{R, \text{inv}}$ is about 5.075 K. For nitrogen, reference 34 gives $T_{R, \text{inv}} = 4.75$ and reference 6 gives $T_{R, \text{inv}} = 4.92$. For argon, reference 6 gives $T_{R, \text{inv}} = 4.8$, and reference 23 gives $T_{R, \text{inv}} = 5.26$.

The Joule or free expansion coefficient

$$\eta \equiv \rho^2 \left(\frac{\partial T}{\partial \rho} \right)_U$$

has an inversion temperature at the maximum in the second virial coefficient B for low densities. While the relation between the Joule-Thomson coefficients φ and μ is simple, the relation to the Joule coefficient is more complex

$$\begin{aligned} \eta C_v &= T \left(\frac{\partial P}{\partial T} \right)_\rho - P \\ &= \rho^2 \left\{ -\varphi + \left[\frac{\partial(P/\rho)}{\partial P} \right]_T \right\} \left(\frac{\partial P}{\partial \rho} \right)_T \end{aligned} \quad (\text{B10})$$

where $\varphi = -\mu C_p$. Substituting equation (B4) into (B10), we find for the region of low pressure (low density) that

$$\frac{\eta C_v}{R \rho^2 T^2} \simeq \frac{dB}{dT} \quad (\text{B11})$$

Note that at zero pressure, η is zero; but for densities low enough for equation (B11) to hold, the Joule coefficient has an inversion where B is a maximum. Values of this inversion temperature, as listed in table I, were obtained from reference 34. B as given by equation (B3) does not possess a maximum for $T \leq 4000$ K. Such temperatures are far beyond the range of the curve fits and beyond the scope of the Joule-Thomson curves for fluids discussed herein. It is also interesting to note that this inversion temperature does not exist for the Van der Waal fluid, as B does not attain a maximum.

The Boyle temperature is that temperature for which the second virial coefficient vanishes, that is, when $B = 0$. The Boyle temperatures are also given in table I. For the Van der Waal fluid, equations (B8) and (B9) give

$$T_{R,B} = \frac{T_{R,inv}}{2} \quad (\text{B12})$$

The relation between calculated and reduced temperatures and the calculated reduced Boyle temperatures seem to follow equation (B12) even though the Van der Waal temperatures T_B and T_{inv} do not.

APPENDIX C

CRITICAL ISENTHALPIC JOULE-THOMSON COEFFICIENT

The specific heat at constant pressure may be written as

$$C_p = C_v + \frac{T \left[\left(\frac{\partial P}{\partial T} \right)_\rho \right]^2}{\rho^2 \left(\frac{\partial P}{\partial \rho} \right)_T} \quad (C1)$$

When this expression for C_p is substituted into equation (1), the isenthalpic Joule-Thomson coefficient becomes

$$\mu = \frac{\frac{T}{\rho} \left(\frac{\partial P}{\partial T} \right)_\rho - \left(\frac{\partial P}{\partial \rho} \right)_T}{\rho \left\{ \left(\frac{\partial P}{\partial \rho} \right)_T C_v + \frac{T}{\rho^2} \left[\left(\frac{\partial P}{\partial T} \right)_\rho \right]^2 \right\}} \quad (C2)$$

Now as one approaches the critical point, the equation of state strongly satisfies

$$\lim_{P \rightarrow P_c, V \rightarrow V_c, T \rightarrow T_c} \left(\frac{\partial P}{\partial \rho} \right)_T = 0 \quad (C3)$$

while the specific heat at constant volume has at most a logarithmic infinity; that is, very slowly approaches ∞ . Thus, the critical isenthalpic Joule-Thomson coefficient becomes

$$\mu_c = \lim_{P \rightarrow P_c, V \rightarrow V_c, T \rightarrow T_c} \mu = \left[\left(\frac{\partial P}{\partial T} \right)_\rho \right]^{-1} \Bigg|_{P_c, V_c, T_c} \quad (C4)$$

Furthermore, multiplying equation (C2) by P/T , using the result of equation (C3), and applying the limit of equation (C4) yields the dimensionless parameter

$$\frac{P_c \mu_c}{T_c} = \lim_{PVT \rightarrow P_c V_c T_c} \frac{P \mu}{T} = \left[\left(\frac{\partial \ln P}{\partial \ln T} \right)_\rho \right]^{-1} \Bigg|_{P_c V_c T_c} \quad (C5)$$

which normalizes the critical isenthalpic Joule-Thomson coefficient μ_c . The value of $(\partial P / \partial T)_\rho$ can be found from references 14 and 15. However, for methane, nitrogen, oxygen, carbon dioxide, and argon Bender (ref. 14) gives a nearly constant value for the product $(T/P)(\partial P / \partial T)_{P_c V_c T_c}$; that is, the normalized critical isenthalpic Joule-Thomson coefficient (eq. (C4)) is nearly a constant,

$$\frac{T_c}{P_c \mu_c} = \left[\left(\frac{\partial \ln P}{\partial \ln T} \right)_\rho \right]_{P_c V_c T_c} = \frac{T_c}{P_c} \left[\left(\frac{\partial P}{\partial T} \right)_\rho \right]_{P_c V_c T_c} \approx 6 \quad (C6)$$

Rearranging μ_c becomes

$$\mu_c \approx \frac{T_c}{6P_c} \quad (C7)$$

The values of μ_c calculated from equation (C7) and from reference 15 for the fluids considered herein are given in table II.

Using μ_c we can find the critical dependency of the isothermal Joule-Thomson coefficient φ and the Joule or free expansion coefficient η . The Joule or free expansion coefficient may be written as

$$\eta C_v = T \left(\frac{\partial P}{\partial T} \right)_\rho - P$$

Rearranging and passing the limit

$$\lim_{PVT \rightarrow P_c V_c T_c} \left(\frac{\eta C_v + P}{P} \right) = \lim_{PVT \rightarrow P_c V_c T_c} \frac{T}{P} \left(\frac{\partial P}{\partial T} \right)_\rho \approx 6$$

and

$$\eta_c = \frac{5P_c}{(C_v)_c}$$

since $(C_v)_c$ is weakly divergent, η_c must approach zero in a weak manner.

The isothermal Joule-Thomson coefficient, from appendix A, is directly related to μ through C_p ,

$$\varphi = -\mu C_p$$

In the critical region, C_p diverges as $|T - T_c|^{-4/3}$, while μ remains finite and non-zero. Consequently, φ_c diverges as C_p , that is,

$$\varphi_c \propto |T - T_c|^{-4/3}$$

APPENDIX D

JOULE-THOMSON LIQUIFIER AND REFRIGERATOR CYCLES AND OPERATING OPTIMUMS

A Joule-Thomson liquifier and refrigerator is illustrated schematically in figures 17 and 18 (see also refs. 19 and 49). The only difference between the two devices is the makeup gas supplied to the liquifier at the compressor; consequently, the temperature-entropy and enthalpy-temperature diagrams apply to either process.

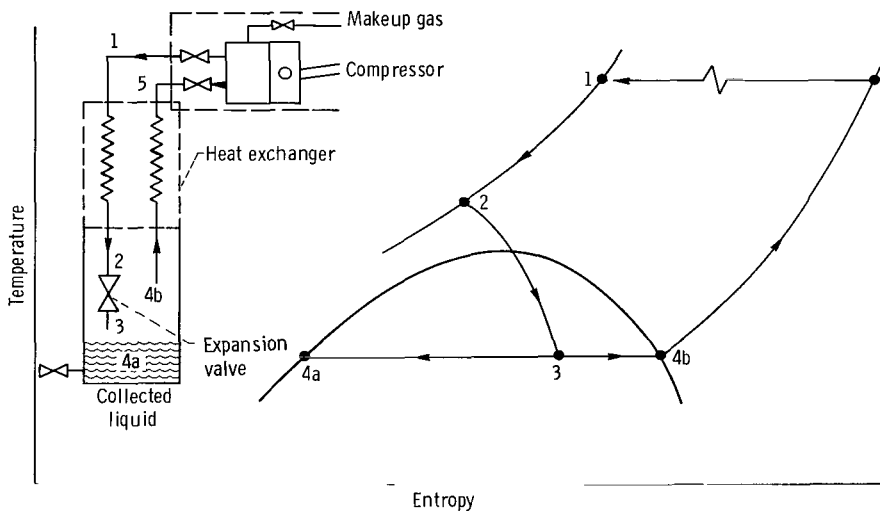


Figure 17. - Process diagram and flow schematic for a Joule-Thomson liquifier. Process diagram also applies to Joule-Thomson refrigerator.

The compressor need not be a part of the cycle; however, high-pressure gas must be supplied and a return provided. The Joule-Thomson process could be the last of several stages in a real refrigerator or liquifier of gas compressed isothermally at ambient temperature T_a to inlet pressure P_1 .

Upon passing through the heat exchanger \dot{m} g/sec of fluid is expanded isenthalpically such that \dot{n} g/sec of the gas are liquified. The energy balance requires

$$\dot{m}H_1 = \dot{n}H_{4a} + (\dot{m} - \dot{n})H_5 \quad (D1)$$

Since we want to maximize the amount of liquid produced and the liquid reservoir pressure is fixed, the only variable at our disposal is H_1 , which is controlled by P_1

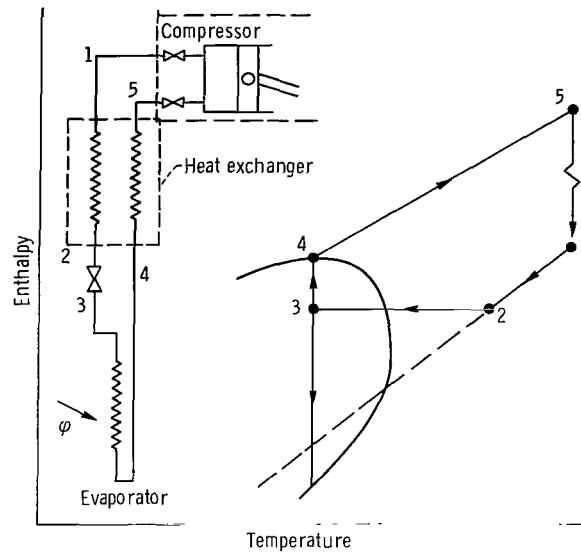


Figure 18. - Process diagram and flow schematic for Joule-Thomson refrigerator. Process diagram also applies to Joule-Thomson liquifier.

$$\frac{\partial \left(\frac{\dot{m}}{\dot{n}} \right)}{\partial P_1} = \left(\frac{\partial H_1}{\partial P_1} \right)_{T=T_a} = 0 \quad (D2)$$

But the latter term is the isothermal Joule-Thomson coefficient. This term is zero only when P and T lie on the inversion curve (appendix A). Consequently, the maximum liquification or refrigeration occurs when the process starts on the inversion curve.

However, the maximum liquification or refrigeration "costs" more than operating on a locus within the Joule-Thomson inversion curve. To see this, again consider the liquifier. If we let η_e represent the efficiency of the compressor, etc., the work required to compress \dot{m} g/sec of gas (isothermally) becomes

$$W_p = \dot{m} R T_a \ln \left(\frac{P_1}{P_5} \right)$$

Dividing by the amount of liquid produced ($\dot{n} \equiv \dot{n}_2$ g/sec) gives a figure of merit for the system. Minimizing the figure of merit with respect to our only variable P_1 gives

$$\frac{\partial \left(\frac{W_p}{\eta_e \dot{n}_2} \right)}{\partial P_1} = 0 = \frac{H_5 - H_1}{P_1} + \left[\ln \left(\frac{P_1}{P_5} \right) \right] \left(\frac{\partial H_1}{\partial P_1} \right)_{T_a} \quad (D3)$$

and from the heat exchanger load,

$$(H_1 - H_2) = \left(1 - \frac{\dot{n}_2}{\dot{m}} \right) (H_5 - H_{4f}) \quad (D4)$$

which represents the second law constraint (heat flow requires a positive temperature difference). Also, it must be noted that the process is constrained to those points where P_3 is less than P_c and μ is less than zero.

Equation (D3) is identical in form to that of Dean and Mann (ref. 19) for Joule-Thomson refrigerators. Note that equation (D4) for the Joule-Thomson liquifier readily reduces to the heat exchanger load for the refrigeration, \dot{n}_2 equals zero. Dean and Mann numerically solved equation (D3) with \dot{n}_2 replaced by \dot{m} and equation (D4) with $[1 - (\dot{n}_2/\dot{m})]$ replaced by unity, for the fluids helium, para-hydrogen, and nitrogen, presenting curves similar to that of figure 19. It is quite apparent that one should operate well within the inversion curve to minimize cost. However, other methods of reducing the operating costs are to add intermediate cycles, as illustrated in figure 20, to pre-cool the inlet gas, or by cascading using second single cycles with different fluids.

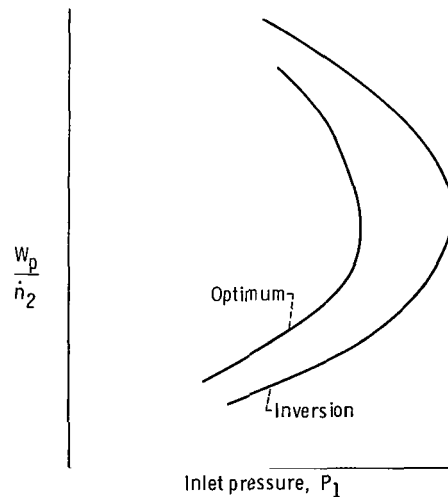


Figure 19. - Comparison of inversion curve and optimum (minimum cost) operating locus for Joule-Thomson processes.

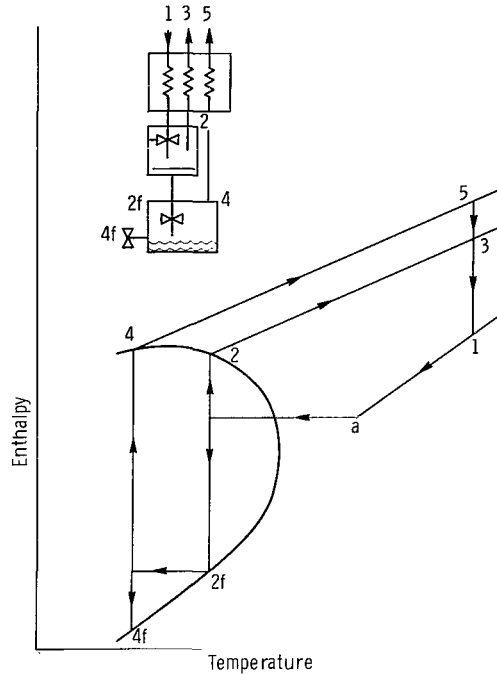


Figure 20. - Double-cascade Joule-Thomson liquifier (early Linde process for air).

The energy balance, isothermal compressor work, and heat exchanger balance become, for $\mu > 0$,

$$\left. \begin{aligned}
 \dot{m}H_1 &= \dot{n}_2H_{2f} + (\dot{m} - \dot{n}_2)H_3 \\
 \dot{n}_2H_{2f} &= \dot{n}_4H_{4f} - (\dot{n}_2 - \dot{n}_4)H_5 \\
 W_p &= RT_a \left(\dot{m} \int_{P_1}^{P_3} \frac{dP}{P} + \dot{n}_2 \int_{P_3}^{P_5} \frac{dP}{P} \right) \\
 \dot{m}(H_1 - H_a) &= (\dot{m} - \dot{n}_2)(H_3 - H_2) + (\dot{n}_2 - \dot{n}_4)(H_5 - H_4)
 \end{aligned} \right\} \quad (D5)$$

Note here that $(\dot{m} - \dot{n}_2)$ represents the mass of gas returning to the compressor and that \dot{n}_2 represents the gas or liquid passing to the second Joule-Thomson valve. Solving for the figure of merit,

$$\frac{W_p}{\dot{n}_4} = RT_a \frac{\ln \frac{P_1}{P_3} + \frac{\dot{n}_2}{\dot{m}} \ln \frac{P_3}{P_5}}{H_3 - H_1 + \frac{\dot{n}_2}{\dot{m}} (H_5 - H_3)} \quad (D6)$$

$$\frac{W_p}{\dot{n}_4} = RT_a \frac{\ln \frac{P_1}{P_3} + \frac{\dot{n}_2}{\dot{m}} \ln \frac{P_3}{P_5}}{H_5 - H_{4f}}$$

This procedure can easily be extended to N-stages

$$\left. \begin{aligned} H_1 &= \frac{\dot{n}_{2N}}{\dot{m}} H_{2N_f} + \frac{1}{\dot{m}} \sum_{k=1}^N (\dot{n}_{2k-2} - \dot{n}_{2k}) H_{2k+1} \\ W_p &= \dot{m} RT_a \sum_{k=0}^{N-1} \dot{n}_{2k} \ln \left(\frac{P_{2k+1}}{P_{2k+3}} \right) \quad \text{where } \dot{n}_0 = \dot{m} \\ \dot{m}(H_1 - H_2) &= \sum_{k=0}^N (\dot{n}_{2k-2} - \dot{n}_{2k}) (H_{2k+1} - H_{2k}) \end{aligned} \right\} \quad (D7)$$

Equations (D7) can be readily solved for the figure of merit for an N-stage Joule-Thomson process,

$$\frac{W_p}{\dot{n}_{2N}} = \frac{RT_a \left[\sum_{k=0}^{N-1} \frac{\dot{n}_{2k}}{\dot{m}} \ln \left(\frac{P_{2k+1}}{P_{2k+3}} \right) \right] (H_{2N_f} - H_{2N+1})}{H_1 - \frac{\dot{n}_{2N-2}}{\dot{m}} H_{2N+1} - \frac{1}{\dot{m}} \sum_{k=0}^{N-1} (\dot{n}_{2k-2} - \dot{n}_{2k}) H_{2k+1}} \quad (D8)$$

The optimization procedure becomes quite complicated and of academic interest. For example, the optimum W_p/\dot{m} in equation (D6) is for \dot{n}_2 equals zero; that is, no fluid passing to the second J-T valve. However, the whole idea is to produce liquid, and the optimum curves are found by plotting those points that can be attained by expanding from P_1 to P_3 . The analysis can, however, serve as a guide to experimental testing.

If one reflects on the previous discussion for a moment, and uses a little intuition along with figure 7, one would anticipate the maximum temperature drop to occur if the

process started at the inversion curve. Furthermore, since most of the curves are quite flat near the inversion curve, one would expect that nearly the same amount of refrigeration could be obtained for a significantly lower pressure drop, at a substantial savings in compressor power.

APPENDIX E

DIFFERENCES IN CARBON MONOXIDE PROPERTIES

The inversion curve of figure 8(g) as calculated from reference 15 and the results of Leah (ref. 29) are in considerable disagreement. As the PVT data from reference 15 are extrapolated considerably beyond the range of data used in the curve fit ($T_R < 2\frac{1}{2}$, $P_R < 9$), a direct comparison of density, enthalpy, entropy, and specific heats was made.

In figure 21(a) the difference in density is plotted as a function of reduced pressure for temperature increments of 100 K. For $T_R < 3$, the difference appears to be about 0.2 ± 0.1 percent, which seems quite good. The shaded band indicates the difference expected at the inversion curve for $T_R > 2$. One part of the band is formed from figure 8(g), the other from the data of Leah (ref. 29). As can be seen, the difference increases as T_R increases to 5 and $P_R \approx 6$. The difference in density along the inversion curve then diminishes as pressure is reduced. Thus, the inversion curve in the region $T_R > 3$ and $1 < P_R < 11\frac{1}{2}$ seems to have a significant departure from that of Leah (ref. 29). However, in figure 8(g), the deviations from Leah (ref. 29) are significant even for $T_R < 3$. Thus, not all the answers lie in the PVT results.

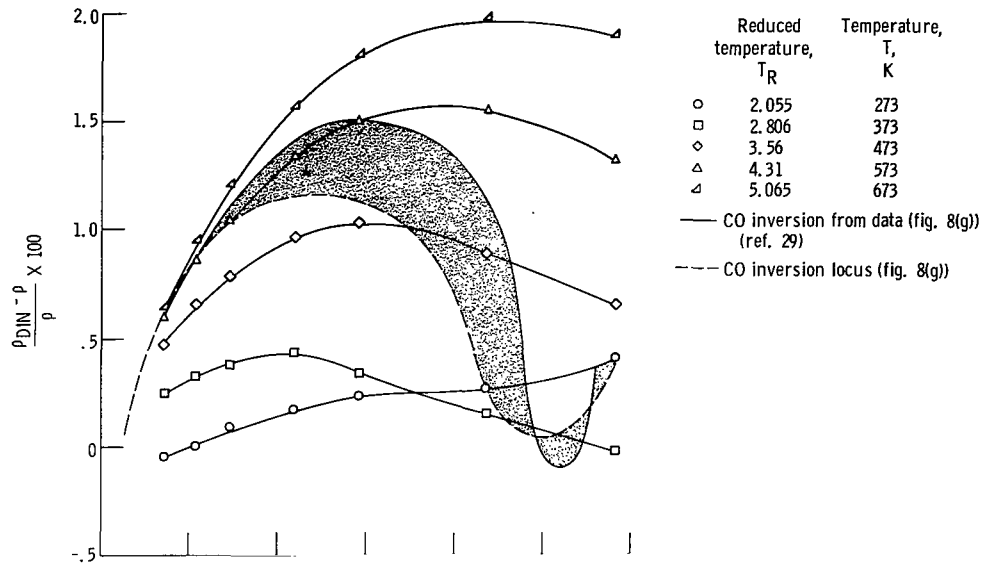
In figure 21(b) the difference in enthalpy along the inversion curve is considerable between $10 < P_R < 12$, passes through a minimum near $P_R = 9$, and increases as pressure decreases. As very small deviations in the enthalpy in this region will significantly alter the inversion locus, it appears that derived properties (i. e., the $(\partial P/\partial T)_\rho$) may be the source of the differences.

However, in figure 21(c) the difference in entropy along the inversion curve is about 0.9 ± 0.2 percent for $P_R < 11$, which apart from the level shift in S_0 is quite reasonable. As both enthalpy and entropy require $(\partial P/\partial T)_\rho$, such agreement tends to exonerate the derivative $(\partial P/\partial T)_\rho$.

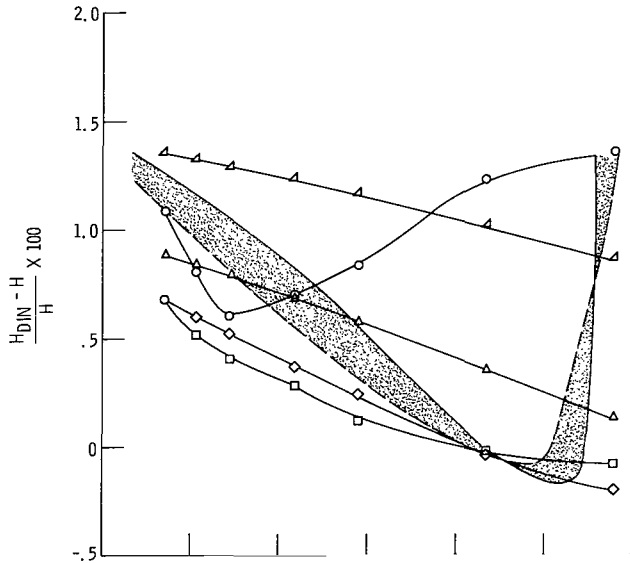
In figure 21(d) the difference in specific heat at constant volume is quite large and directly related to temperature level. Even in the regime where the results of reference 15 are quite accurate ($T_R < 2\frac{1}{2}$) the differences are large. This, however, would only tend to implicate $\partial^2 P/\partial T^2$, which is a troublesome point in many a curve fit and sheds little light here, as either (or both) references 15 or 29 could be in error.

In figure 21(e) the differences in specific heat at constant pressure along the inversion curve are, as were C_v errors, a function of temperature level. However, superposition of the two difference curves indicates them to be equivalent, except at $T_R < 3$. As C_p is determined from C_v and the partials $(\partial P/\partial T)_\rho$ and $(\partial P/\partial \rho)_T$ seem valid, C_p appears to be within the limits of uncertainty in $(\partial^2 P/\partial T^2)$.

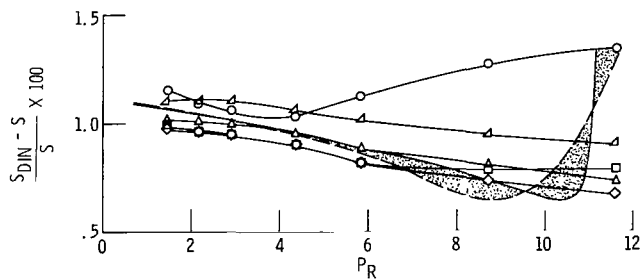
Consequently, it would appear that the variations in density coupled with the varia-



(a) Relative density differences.



(b) Relative enthalpy differences.



(c) Relative entropy differences.

Figure 21. - Comparison of carbon monoxide properties as calculated from reference 15 with those of reference 29, at several reduced pressures for selected isotherms. Expected differences along inversion curves (Leah's results vs. ref. 15) are bounded by shaded region.

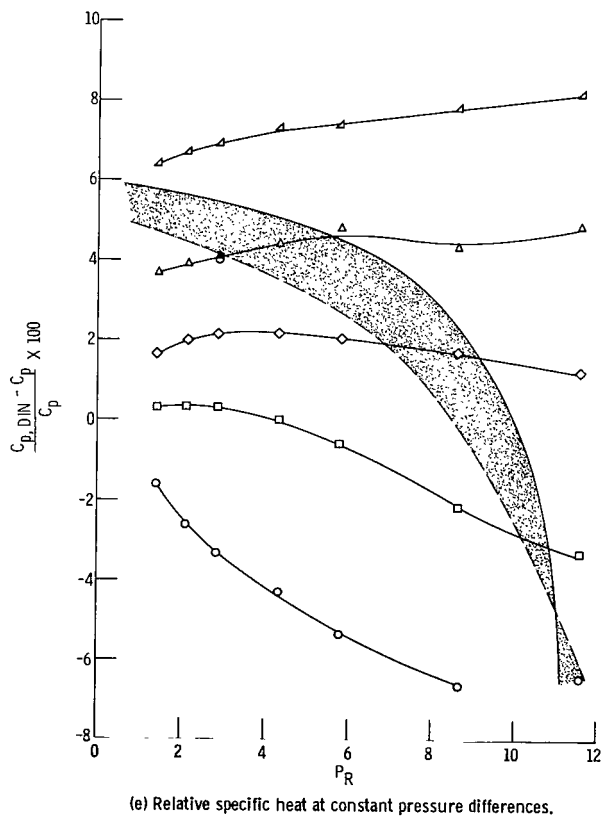
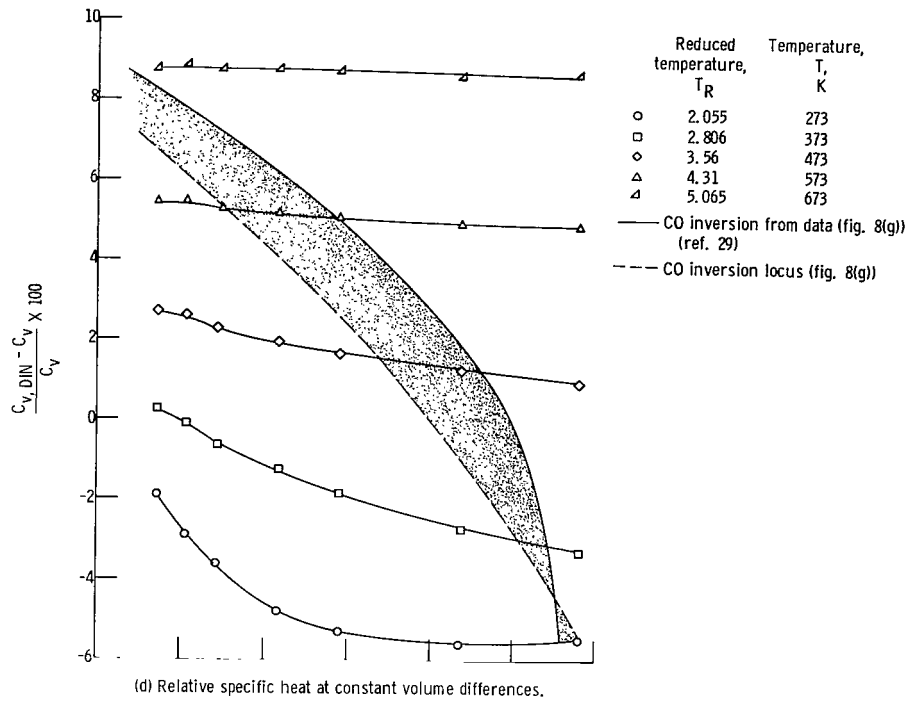


Figure 21. - Concluded.

tions in $(\partial P/\partial T)_\rho$ lead to small shifts in the isenthalps, which in turn lead to deviations in the inversion curve. However, the data of Michels, Lunbeck, and Wolkers (ref. 30) depart significantly from those of Leah (ref. 29) and to a lesser extent from the results of reference 15. But these data appear to follow a curve about 5 percent higher than the inversion curve of figure 8(g) and 10 percent lower than that of Leah (ref. 29).

It is quite apparent that the carbon monoxide data need to be reevaluated and a new equation of state presented.

Finally, invoking the principle of corresponding states, one would expect the inversion curve to more closely follow that of Leah (ref. 29). Therefore, the curve of figure 8(g) should be considered valid for $T_R < 3$ and low for $T_R \geq 3$.

APPENDIX F

SYMBOLS

$A(T), B(T), C(T), D(T),$ $E(T), F(T), G(T), H(T)$	temperature functions in equation of state of ref. 15
$A_{0, 1, . . . 6}$	constants
a, b	constants in Van der Waal equation of state
B	second virial coefficient
B'	modified second virial coefficient
C	third virial coefficient
C'	modified third virial coefficient
C_p	specific heat at constant pressure, J/(g)(K)
C_v	specific heat at constant volume, J/(g)(K)
D	fourth virial coefficient
H	enthalpy, J/g
k	summation index
\dot{m}	mass flow rate, g/sec
N	number of stages
n	number of points
\dot{n}	mass flow rate, g/sec
n_i	constants in equation of state (ref. 15) as modified to accommodate ref. 13 ($i = 1, 2, 3, 4, 5 . . . 20, 21, 25$)
P	pressure, MN/m ²
R	gas constant, J/(g)(K)
S_0	reference entropy, J/(g)(K)
U	internal energy, J/g
V	specific volume, cm ³ /g
W_p	compressor or pump work, J/(sec)(W)
T	temperature, K
T_2	temperature, used in helium fit only, K

Z	compressibility factor, PV/RT
α_i	constants ($i = 1, 2, \dots, 5$)
β_i	constants ($i = 1, 2, \dots, 7$)
ρ	density, g/cm^3
φ	isothermal Joule-Thomson coefficient, cm^3/g
η	Joule or free expansion coefficient, $(g)(K)/cm^3$
η_e	efficiency
μ	isenthalpic Joule-Thomson coefficient, $K/(MN)(m^2)$
ω	acentric factor, $\approx - \left[\left(1 + \log_{10} P_{R, vp} \right)_{T_R=0.7} \right]$ (ref. 50)

Subscripts:

a	ambient
B	Boyle
c	critical
data	data
inv	inversion
f	liquid
max	maximum
N_2	nitrogen
R	reduced
vp	vapor pressure
0	zero pressure
1, 2, 3 . . .	states on thermodynamic diagram

Superscripts:

0	pseudovalue
'	(see fig. 9)

REFERENCES

1. Timmerhaus, K. D., ed.: *Advances in Cryogenic Engineering*. Vol. 15. Plenum Press, 1970, sections K and L, pp. 415-475.
2. Roebuck, J. R.; and Osterberg, H.: The Joule-Thomson Effect in Helium. *Phys. Rev.*, vol. 43, no. 1, Jan. 1, 1933, pp. 60-69.
3. Roebuck, J. R.; and Osterberg, H.: The Thermodynamic Properties of Helium Gas. *Phys. Rev.*, vol. 45, no. 5, Mar. 1, 1934, pp. 332-340.
4. Roebuck, J. R.; and Osterberg, H.: The Joule-Thomson Effect in Argon. *Phys. Rev.*, vol. 46, no. 9, Nov. 1, 1934, pp. 785-790.
5. Roebuck, J. R.; and Osterberg, H.: The Joule-Thomson Effect in Nitrogen. *Phys. Rev.*, vol. 48, no. 5, Sept. 1, 1935, pp. 450-457.
6. Roebuck, J. R.; and Osterberg, H.: The Joule-Thomson Effect in Mixtures of Helium and Nitrogen. *J. Am. Chem. Soc.*, vol. 60, no. 2, Feb. 1938, pp. 341-351.
7. Roebuck, J. R.; and Osterberg, H.: The Joule-Thomson Effect in Mixtures of Helium and Argon. *J. Chem. Phys.*, vol. 8, no. 8, Aug. 1940, pp. 627-635.
8. Jakob, M.: Inversion Curve of the Joule-Thomson Effect in Gases. *Phys. Zeit.*, vol. 22, Feb. 1, 1921, pp. 65-69.
9. Watson, K. M.; and Smith, R. L.: Generalized High Pressure Properties of Gases. *Nat. Petroleum News*, vol. 28, no. 27, July 1, 1936, pp. 29-30, 34-36.
10. Gunn, R. D.; Chueh, P. L.; and Prausnitz, J. M.: Inversion Temperatures and Pressures for Cryogenic Gases and Their Mixtures. *Cryogenics*, vol. 6, no. 6, Dec. 1966, pp. 324-329.
11. Vennix, Alan J.: Low Temperature Volumetric Properties and the Development of an Equation of State for Methane. Ph.D. Thesis, Rice University, 1966.
12. Weber, L. A.: Thermodynamics and Related Properties of Oxygen from the Triple Point to 300 K at Pressures to 330 Atmospheres. Rep. 9710, National Bureau of Standards (NASA CR-99159), June 20, 1968.
13. Coleman, T. C.; and Stewart, R. B.: Thermodynamic Properties of Nitrogen from 70 K to 1000 K with Pressures to 1000 Atm. Presented at the NAS-NRC 13th International Congress of Refrigeration, Washington, D.C., Aug. 27-Sept. 3, 1971.

14. Bender, E.: Equations of State Exactly Representing the Phase Behavior of Pure Substances. Proceedings of the Fifth Symposium on Thermophysical Properties. ASME, 1970, pp. 227-235.
15. Hendricks, R. C.; Baron, A.; Peller, I.; and Pew, K. J.: GASP - A Computer Code for Calculating the Thermodynamic and Transport Properties for Eight Fluids - Helium, Methane, Neon, Nitrogen, Carbon Monoxide, Oxygen, Argon, Carbon Dioxide. Presented at the NAS-NRC 13th International Congress of Refrigeration, Washington, D. C., Aug. 27-Sept. 3, 1971.
16. Deming, W. Edwards; and Shupe, Lola E.: Some Physical Properties of Compressed Gases. I. Nitrogen. Phys. Rev., vol. 37, no. 5, Mar. 1, 1931, pp. 638-654.
17. Deming, Edwards W.; and Deming, Lola S.: Some Physical Properties of Compressed Gases. V. The Joule-Thomson Coefficient for Nitrogen. Phys. Rev., vol. 48, no. 5, Sept. 1, 1935, pp. 448-449.
18. Lunbeck, R. J.; Michels, A.; and Wolkers, G. J.: Thermodynamic Properties of Nitrogen as Functions of Pressure and Temperature Between 0 and 6000 Atmospheres and -125° and $+150^{\circ}$ C. Appl. Sci. Res., vol. A3, 1952, pp. 197-210.
19. Dean, J. W.; and Mann, D. B.: The Joule-Thomson Process in Cryogenic Refrigeration Systems. Tech. Note 227, National Bureau of Standards, Feb. 14, 1965.
20. Din, F.: Nitrogen. Thermodynamic Functions of Gases. Vol. 3. F. Din, ed., Butterworth, Inc., 1961, pp. 72-161.
21. Gunn, R. D.; Chueh, P. L.; and Prausnitz, J. M.: Prediction of Thermodynamic Properties of Dense Gas Mixtures Containing One or More of the Quantum Gases. AIChE J., vol. 12, no. 5, Sept. 1966, pp. 937-941.
22. Tester, H. E.: Methane. Thermodynamic Functions of Gases. Vol. 3. F. Din, ed., Butterworth, Inc., 1961, pp. 1-71.
23. Grossman, A. L.; McCarty, R. D.; and Hust, J. G.: Thermodynamic Properties of Argon from the Triple Point to 300 K at Pressures to 1000 Atmospheres. Rep. NSRDS-NBS-27, National Bureau of Standards (NASA CR-100532), Mar. 1969.
24. Michels, A.; Levelt, J. M.; and Wolkers, G. J.: Thermodynamic Properties of Argon at Temperatures Between 0° C and -140° C and at Densities up to 640 Amagat (Pressures up to 1050 atm.). Physica, vol. 24, 1958, pp. 769-794.
25. Michels, A.; Lunbeck, R. J.; and Wolkers, G. J.: Thermodynamical Properties of Argon as Function of Density and Temperature Between 0° and 150° C and Densities to 640 Amagat. Physica, vol. 15, 1949, pp. 689-695.

26. Michels, A.; Lunbeck, R. J.; and Wolkers, G. J.: Thermodynamical Properties of Argon as Function of Pressure and Temperature Between 0 and 2000 Atmospheres and 0^o and 150^o C. *Appl. Sci. Res.*, vol. A2, 1951, pp. 345-350.
27. Roebuck, J. R.; Murrell, T. A.; and Miller, E. E.: The Joule-Thomson Effect in Carbon Dioxide. *J. Am. Chem. Soc.*, vol. 64, no. 2, Feb. 1942, pp. 400-411.
28. Newitt, D. M.; Pai, M. V.; Kuloor, N. R.; and Huggill, J. A. W.: Carbon Dioxide. *Thermodynamic Functions of Gases*. Vol. 1. F. Din, ed., Butterworth, Inc., 1956.
29. Leah, A. Smeeton: Carbon Monoxide. *Thermodynamic Functions of Gases*. Vol. 1. F. Din, ed., Butterworth, Inc., 1956.
30. Michels, A.; Lunbeck, R. J.; and Wolkers, G. J.: Thermodynamic Properties of Carbon Monoxide at Temperatures Between 0 and 150 C and at Pressures up to 3000 Atmospheres. *Appl. Sci. Res.*, vol. A3, 1952, pp. 253-260.
31. Baehr, Hans D.: Zur Kenntnis des Joule-Thomson-Effekts und der Molwärme von Deuterium und Helium. *Z. Electrochem.*, vol. 60, no. 5, 1956, pp. 515-517.
32. Keesom, Willem H.: Helium. Elsevier Publ. Co., 1942.
33. Hill, R. W.; and Lounasmaa, O. V.: The Thermodynamic Properties of Fluid Helium. *Phil. Trans. Roy. Soc., Ser. A*, vol. 252, no. 1013, Mar. 31, 1960, pp. 357-395.
34. Beattie, James A.: Thermodynamics and Physics of Matter. Vol. 1 of High Speed Aerodynamics and Jet Propulsion. Frederick D. Rossini, ed., Princeton University Press, 1955, p. 249.
35. Keyes, Frederick G.: Gas Thermometer Scale Corrections Based on an Objective Correlation of Available Data for Hydrogen, Helium and Nitrogen. *Temperature, Its Measurement and Control in Science and Industry*. Reinhold Publ. Corp., 1941, pp. 45-59.
36. Kirkwood, John G.; and Keyes, Frederick G.: The Equation of State of Helium. *Phys. Rev.*, vol. 37, no. 7, Apr. 1, 1931, pp. 832-840.
37. Crawford, Franz H.: Heat, Thermodynamics, and Statistical Physics. Harcourt, Brace & World, 1963.
38. Mann, Douglas B.: The Thermodynamic Properties of Helium from 3 to 300^o K Between 0.5 and 100 Atmospheres. Tech. Note 154, National Bureau of Standards, Jan. 1962.
39. Goldberg, Fredric N.; and Haferd, Angela M.: Numerical Procedures for Calculating Real Fluid Properties of Normal and Parahydrogen. NASA TN D-4341, 1968.

40. Roder, H. M.; Weber, L. A.; and Goodwin, R. D.: Thermodynamic and Related Properties of Para-Hydrogen from the Triple Point to 100^o K at Pressures to 340 Atmospheres. Monograph 94, National Bureau of Standards (NASA CR-64443), Aug. 10, 1965.
41. Michels, A.; DeGraaff, W.; and Wolkers, G. J.: Thermodynamic Properties of Hydrogen and Deuterium at Temperatures Between -175^o C and 150^o C and at Densities up to 840 Amagat. *Physica*, vol. 25, 1959, pp. 1097-1124.
42. McCarty, R. D.; and Stewart, R. B.: Thermodynamic Properties of Neon from 25 to 300^o K Between 0.1 and 200 Atmospheres. *Advances in Thermophysical Properties at Extreme Temperatures and Pressures*. Serge Gratch, ed., ASME, 1965, pp. 84-97.
43. Michels, A.; and Gibson, R. O.: Measurements of Isothermals (of Neon) at High Pressures. *Ann. d. Physik*, vol. 87, Nov. 22, 1928, pp. 850-876.
44. Trappeniers, N. J.; Wassenaar, T.; and Wolkers, G. J.: Isotherms and Thermodynamic Properties of Krypton at Temperatures Between 0^o and 150^o C and at Densities up to 620 Amagat. *Physica*, vol. 32, 1966, pp. 1503-1520.
45. Michels, A.; Wassenaar, T.; Wolkers, G. J.; and Dawson, J.: Thermodynamic Properties of Xenon as a Function of Density up to 520 Amagat and as a Function of Pressure up to 2800 Atmospheres, at Temperatures Between 0^o C and 150^o C. *Physica*, vol. 22, 1956, pp. 17-28.
46. Prydz, Rolf; and Straty, G. C.: PVT Measurements, Virial Coefficients, and Joule-Thomson Inversion Curve of Fluorine. *J. Res. Nat. Bur. Standards, Sec. A - Phys. Chem.*, vol. 74A, no. 6, Nov.-Dec. 1970, pp. 747-760.
47. Ruhemann, M.; and Ruhemann, B.: *Low-Temperature Physics*. Cambridge University Press, 1937.
48. Francis, P. G.; and Luckhurst, G. R.: Joule-Thomson Coefficients and the Principle of Corresponding States. *Trans. Faraday Soc.*, vol. 59, 1963, pp. 667-672.
49. Faires, Virgil M.: *Elementary Thermodynamics*. Third ed., Macmillan Co., 1957.
50. Reid, Robert C.; and Sherwood, Thomas K.: *The Properties of Gases and Liquids: Their Estimation and Correlation*. Second ed., McGraw-Hill Book Co., Inc., 1966.

BIBLIOGRAPHY

- Budenholzer, R. A.; Sage, B. H.; and Lacey, W. N.: Phase Equilibria in Hydrocarbon Systems. Joule-Thomson Coefficient of Methane. *Ind. Eng. Chem.*, vol. 31, no. 3, Mar. 1939, pp. 369-374.
- DeGroot, S. R.; and Geldermans, M.: The Joule-Thomson Effect in Ethylene. *Physica*, vol. 13, 1947, pp. 538-542.
- Johnston, H. L.; and White, David: VII - A Summary of Experimental Determinations of Joule-Thomson Effects in Gases. *Trans. ASME*, vol. 70, no. 6, Aug. 1948, pp. 651-654.
- Meissner, W.: Erzeugung tiefer Temperaturen und Gasverflüssigung. *Handbuch der Physik*, 11, 1926. Referenced in Ruhemann, M. and B.: *Low-Temperature Physics*. Cambridge University Press, 1937, p. 20.
- Sage, B. H.; Webster, D. C.; and Lacey, W. N.: Phase Equilibria in Hydrocarbon Systems. XVIII. Thermodynamic Properties of Ethane. *Ind. Eng. Chem.*, vol. 29, no. 6, June 1937, pp. 658-666.
- Whalley, E.: Thermodynamic Properties of Argon in the Temperature Range -100 to +600^o C. and Pressure Range 0 to 80 Atmospheres. *Can. J. Tech.*, vol. 33, 1955, pp. 111-116.



011 001 C1 U 33 720630 S00903DS
DEPT OF THE AIR FORCE
AF WEAPONS LAB (AFSC)
TECH LIBRARY/WLOL/
ATTN: E LOU BOWMAN, CHIEF
KIRTLAND AFB NM 87117

POSTMASTER: If Undeliverable (Section 15
Postal Manual) Do Not Return

"The aeronautical and space activities of the United States shall be conducted so as to contribute . . . to the expansion of human knowledge of phenomena in the atmosphere and space. The Administration shall provide for the widest practicable and appropriate dissemination of information concerning its activities and the results thereof."

— NATIONAL AERONAUTICS AND SPACE ACT OF 1958

NASA SCIENTIFIC AND TECHNICAL PUBLICATIONS

TECHNICAL REPORTS: Scientific and technical information considered important, complete, and a lasting contribution to existing knowledge.

TECHNICAL NOTES: Information less broad in scope but nevertheless of importance as a contribution to existing knowledge.

TECHNICAL MEMORANDUMS: Information receiving limited distribution because of preliminary data, security classification, or other reasons.

CONTRACTOR REPORTS: Scientific and technical information generated under a NASA contract or grant and considered an important contribution to existing knowledge.

TECHNICAL TRANSLATIONS: Information published in a foreign language considered to merit NASA distribution in English.

SPECIAL PUBLICATIONS: Information derived from or of value to NASA activities. Publications include conference proceedings, monographs, data compilations, handbooks, sourcebooks, and special bibliographies.

TECHNOLOGY UTILIZATION PUBLICATIONS: Information on technology used by NASA that may be of particular interest in commercial and other non-aerospace applications. Publications include Tech Briefs, Technology Utilization Reports and Technology Surveys.

Details on the availability of these publications may be obtained from:

SCIENTIFIC AND TECHNICAL INFORMATION OFFICE

NATIONAL AERONAUTICS AND SPACE ADMINISTRATION

Washington, D.C. 20546